Physics of Fluids

Steady-state multiple near resonances of periodic interfacial waves with rigid boundary

Cite as: Phys. Fluids **32**, 087104 (2020); https://doi.org/10.1063/5.0015581
Submitted: 29 May 2020 . Accepted: 20 July 2020 . Published Online: 06 August 2020

Jiyang Li (李李阳), Zeng Liu (刘曾), Shijun Liao (廖世俊), and Alistair G. L. Borthwick

Physics of Fluids ARTICLE scitation.org/journal/phf

Steady-state multiple near resonances of periodic interfacial waves with rigid boundary

Cite as: Phys. Fluids 32, 087104 (2020); doi: 10.1063/5.0015581
Submitted: 29 May 2020 • Accepted: 20 July 2020 •
Published Online: 6 August 2020

View Online Export Citation CrossMark

Jiyang Li (李季阳),[1,a)] Zeng Liu (刘曾),[2,3,4,b)] Shijun Liao (廖世俊),[1,4,5,c)] and Alistair G. L. Borthwick[6,d)]

AFFILIATIONS

[1] School of Naval Architecture, Ocean and Civil Engineering, Shanghai Jiao Tong University, Shanghai 200240, China
[2] School of Naval Architecture and Ocean Engineering, Huazhong University of Science and Technology, Wuhan 430074, China
[3] Hubei Provincial Engineering Research Center of Data Techniques and Supporting Software for Ships, Wuhan, Hubei 430074, China
[4] Collaborative Innovative Center for Advanced Ship and Deep-Sea Exploration, Shanghai 200240, China
[5] State Key Laboratory of Ocean Engineering, Shanghai 200240, China
[6] School of Engineering, University of Edinburgh, Edinburgh EH9 3FB, United Kingdom

[a)] **Electronic mail:** lijiyang19930511@sjtu.edu.cn
[b)] **Author to whom correspondence should be addressed:** z_liu@hust.edu.cn
[c)] **Electronic mail:** sjliao@sjtu.edu.cn. **URL:** http://sjliao.sjtu.edu.cn
[d)] **Electronic mail:** Alistair.Borthwick@ed.ac.uk

ABSTRACT

Steady-state resonant interfacial waves in a two-layer fluid within a frictionless duct are investigated theoretically. A combination of the homotopy analysis method (HAM) and Galerkin's method is used to search for accurate steady-state resonant solutions with multiple near resonances. In the HAM, a piecewise parameter in the auxiliary linear operators is introduced to remove the small divisors caused by nearly resonant components. Convergent series solutions are then provided to the Galerkin iterations to accelerate the convergence rate. It is found that weakly nonlinear steady-state resonant waves form a continuum in the parameter space. As nonlinearity (wave steepness) increases, energy appears to be progressively shifted to sideband frequency components, effectively broadening the spectrum. The corresponding interfacial wave profile exhibits an almost fixed spatial pattern of repeated relatively high frequency, high-amplitude bursts followed by low-amplitude, longer waves. On examining the influence of density ratio, though changing slightly, the upper layer enlarges the amplitude of components near primary ones, which reduces the amplitude of higher frequency components, enlarges the wave steepness, and reduces the horizontal velocity in the wave field. Our results indicate that steady-state systems with resonant interactions among periodic interfacial wave components could occur naturally in the ocean. All these should enhance our understanding of periodic resonant interfacial waves.

I. INTRODUCTION

The subsea is a habitat for marine mammals, fish, plankton, and other organisms and also provides a location and working environment for many man-made devices, including submarines, deep sea risers, and elements of offshore structures. Autonomous underwater vehicles are nowadays routinely used for ocean exploration tasks including marine environmental monitoring, seabed mapping, and the mapping and exploitation of submarine resources [see, e.g., Leonard *et al.* (1998) and Leonard and Bahr (2016)]. Internal waves commonly occur in the ocean owing to density stratification caused by temperature or salinity differences. They are believed to provide a transport mechanism for planktonic larvae and also to create so-called dead water zones that hinder ship propulsion.

Internal waves have been studied for decades [see, e.g., Garrett and Munk (1979), Sutherland (2010), and Dauxois *et al.* (2018)]. Hunt (1961) derived a third-order approximation of progressive interfacial waves and considered the effect of upper fluid layer on the wave field. A general theoretical treatment of long internal waves, including solitary and periodic waves, was proposed by Benjamin (1966; 1967). Holyer (1979) studied large amplitude, progressive interfacial waves moving between two infinite fluids of different densities. The Garrett–Munk internal wave spectrum accurately estimated the internal wave energy spectra of most oceanic observations [see Garrett and Munk (1975)]. There have been many field observations of solitary internal waves. For example, Osborne and Burch (1980) reported observations of internal solitons in the Andaman Sea. In recent years, solitary internal waves [see, e.g., Aghsaee *et al.* (2010) and Grimshaw and Helfrich (2012)] and periodic internal waves [see, e.g., Chen and Forbes (2008) and Camassa *et al.* (2010)] have been further investigated through mathematical analysis, numerical simulation, and physical experiments. Although fewer studies have considered periodic internal waves than solitary internal waves owing to the practical difficulties encountered in conducting field observation campaigns and laboratory experiments, research into periodic internal waves is rather important, especially given that the periodic progressive internal waves in the layered fluids constitute a well-documented phenomenon [see, e.g., Holyer (1979), Saffman and Yuen (1982), and Chen and Forbes (2008)].

Interactions among periodic waves can cause resonance, a topic that has been extensively researched in the context of surface gravity waves. The earliest study on surface wave resonance was undertaken by Phillips (1960) who derived the exact resonance criterion for a quartet of periodic progressive waves as

$$\boldsymbol{k}_1 \pm \boldsymbol{k}_2 \pm \boldsymbol{k}_3 \pm \boldsymbol{k}_4 = 0, \quad \omega_1 \pm \omega_2 \pm \omega_3 \pm \omega_4 = 0, \tag{1}$$

where $\boldsymbol{k}_i$ is the wave vector and ω_i is the associated linear angular frequency, with $i = 1, \ldots, 4$. Phillips (1960) found that the amplitude of the resonant wave component increases linearly with time. Another resonant fluid flow topic concerns resonant gravity-driven films on wavy topographies. Linear and nonlinear resonances of viscous films on an oblique wavy plane were studied by Wierschem *et al.* (2008) and Heining *et al.* (2009). The stabilities of film flows over topography were analyzed by Schörner *et al.* (2015) and Aksel and Schörner (2018). Investigations into wave resonance have also extended to periodic internal gravity waves in continuous stratification and interfacial waves in discontinuous layered fluids. Studies of internal wave resonance include the rate of energy transfer in the Garrett–Munk spectra [see, e.g., Mccomas and Bretherton (1977)], collisions of internal wave beams in a uniformly stratified fluid [e.g., Akylas and Karimi (2012)], an instability mechanism causing resonant harmonic generation of internal gravity waves [see, e.g., Liang *et al.* (2017)], and nearly resonant flow at the long-wavelength weakly nonlinear limit in a stratified fluid over topography [see, e.g., Grimshaw and Smyth (1986) and Zhang *et al.* (2008)]. Studies of interfacial wave resonance in a two-layer fluid include Bragg resonance between surface-interfacial waves and a rippled bed [see, e.g., Alam *et al.* (2009)], wave resonance between an "internal" mode and an "external" mode whose dispersion relation is the same as for surface waves, each with the same phase speed but one having twice the wavelength of the other [see, e.g., Parau and Dias (2001)], and triad resonances among surface and interfacial waves [e.g., Ball (1964), Thorpe (1966), Wen (1995), Alam (2012), Tanaka and Wakayama (2015), and Zaleski *et al.* (2019)]. To date, research into triad and higher-order interfacial wave resonances, including surface–interfacial waves and interfacial–interfacial waves, all concerns wave systems with unsteady-state amplitudes that change slowly, vary in the form of Jacobian elliptic functions, or have other relationships changing with time.

In recent years, in the field of surface gravity waves, by using the homotopy analysis method (HAM) (Liao, 2003; 2011a; and Vajravelu and Van Gorder, 2012), Liao (2011b) successfully overcame the problem of singularities identified by Madsen and Fuhrman (2012) and obtained a single steady-state resonant quartet in deep water when condition (1) is exactly satisfied. Xu *et al.* (2012) and Liu and Liao (2014) then found that a steady-state resonant quartet could exist in water of finite depth and for more complicated cases. Similar results concerning the weakly nonlinear steady-state resonant quartet in water of finite depth have also been deduced from Zakharov's equation (Xu *et al.*, 2012). In addition, using model basin tests, Liu *et al.* (2015) experimentally verified the existence of the surface wave systems discovered by Liao (2011b).

Although the foregoing theoretical analyses were based on an exact resonance criterion, there exist near-resonance criteria that are more generalized in their nature than the exact criterion. Without loss of generality, we consider a surface wave system with L nearly resonant components ($\boldsymbol{k}_{0,1}, \boldsymbol{k}_{0,2}, \ldots, \boldsymbol{k}_{0,L}$) derived from two primary components ($\boldsymbol{k}_1, \boldsymbol{k}_2$). It satisfies the following near-resonance criteria:

$$m_l\boldsymbol{k}_1 + n_l\boldsymbol{k}_2 = \boldsymbol{k}_{0,l}, \quad m_l\omega_1 + n_l\omega_2 = \omega_{0,l} + d\omega_{0,l}, \quad l = 1, 2, \ldots, L, \tag{2}$$

where m_l and n_l are integers associated with the lth nearly resonant component, $\boldsymbol{k}_{0,l}$ is the wave vector, $\omega_{0,l}$ is the corresponding linear angular frequency, and $d\omega_{0,l}$ is the angular frequency mismatch (a small real number). Note that the exact resonance can be regarded as a special case of near resonance, but with $d\omega_{0,i} = 0$. As Madsen and Fuhrman (2012) rightly pointed out, setting $d\omega_{0,i} = 0$ causes singularities and inevitably setting $d\omega_{0,i} \approx 0$ for nearly resonant components would lead to very small denominators in the perturbation theory [see, e.g., Liao *et al.* (2016)]. In the framework of the HAM, Liao *et al.* (2016) developed an approach that successfully overcame this problem for a single nearly resonant quartet when $L = 1$ in (2) and obtained solutions for steady-state surface gravity waves in deep water. Liu *et al.* (2017; 2018) and Liu and Xie (2019) extended the method to multiple near resonances when $L > 1$ in (2) and obtained finite amplitude steady-state surface wave systems in any arbitrary water depth. Meanwhile, steady-state resonant solutions for acoustic-gravity waves were also derived by Yang *et al.* (2018) using the HAM.

Unlike the unsteady-state system, there is no energy transfer between the various wave components in the steady-state resonant waves. In the case of unsteady-state resonance, time-dependent periodic exchange of wave energy may happen and the nonlinear wave system would exhibit a Fermi–Pasta–Ulam recurrence phenomenon (Lake *et al.*, 1977). Amundsen (1999) investigated the differences that arise in weakly nonlinear wave resonant interactions under the assumption of a discrete or continuous spectrum. Couston (2016) found that surface waves or internal waves propagating over seabed corrugations can become trapped or deflected. In the case of steady-state resonance, the amplitude of each component is invariant over time. Therefore, the steady-state resonance represents a balanced state of wave energy and is a special case of the more general unsteady-state resonance, where wave energy transfers dynamically among different wave components. Alam *et al.* (2010) pointed out that the dynamic evolution of the wave spectrum with multiple resonances after a long time is complicated and intractable by traditional perturbation methods. Steady-state resonance provides a way to study the evolution of a complex wave system because the components in unsteady-state resonance are hard to distinguish after long-term evolution with the complicated wave generation and transformation. Besides, steady-state resonance could also be regarded as a benchmark to test the accuracy of any numerical algorithm for predicting the long-term evolution of wave systems. Knowledge of steady-state resonant systems provides insight into the behavior of nonlinear interfacial wave evolution. To the best of the authors' knowledge, a system containing resonant interactions among periodic interfacial gravity waves with time-independent amplitudes has not previously been identified.

The objective of this paper is to investigate steady-state resonant interfacial waves with rigid boundaries. A two-layer fluid within a frictionless duct of finite depth is considered. The assumption of a rigid top boundary holds for the following reason: Resonant interactions among surface waves and interface waves are quite complicated to evaluate because multiple external and internal modes of the surface and interface waves have to be considered. When the depth of the upper fluid layer is sufficiently large, the influence of the surface on the interface can be ignored. Therefore, we consider a large depth of the upper fluid layer to simplify the problem to one of interface waves traveling under a rigid top boundary. Physical parameters simplified from data in northeast of the South China Sea (21°N, 118.5°E) (Fan *et al.*, 2013) are used to simulate the actual ocean environment. As a well-established analytical approximation method for nonlinear differential problems, especially in the field of steady-state resonant surface waves, the HAM is used in the present work to derive the steady-state resonant solutions of interfacial waves to a certain level of accuracy. The resulting solutions are then taken as the initial conditions for iteration in Galerkin's method [e.g., Okamura (2010) and Liu and Xie (2019)] to obtain convergent solutions of sufficient accuracy.

The contributions of this paper are summarized as follows: First, the existence of steady-state resonant interfacial waves is confirmed theoretically. It mainly extends the work of Hunt (1961) from progressive interfacial waves with a single primary component to wave groups with two primary components that contain multiple resonances and also extends the work of Liu and Xie (2019) from steady-state resonant surface waves to steady-state resonant interfacial waves. Second, accurate solutions of interfacial waves are obtained in circumstances similar to that of the real ocean environment. The influence of periodic interfacial wave groups on underwater vehicles could be estimated. Finally, the effects of nonlinearity and density ratio on the physics of interfacial wave groups are analyzed. The continuum of the steady-state resonant interfacial waves in the parameter space is established. This work aims to push forward the existence of steady-state resonant waves to more general situations. We believe steady-state resonance can occur for any kind of water wave if resonant interactions among different wave components appear.

This paper is structured as follows: Section II outlines the mathematical derivation. Section III presents the results for linear resonance analysis, weakly nonlinear waves with a single exactly resonant quartet, multiple nearly resonant waves of increased nonlinearity, and resonant waves with different density ratios. Section IV summarizes the main conclusions.

II. MATHEMATICAL FORMULAS

A. Governing equations

Let us consider a system of two incompressible fluid layers, each of constant density under gravity that entirely fills a frictionless duct. Following Alam (2012) and Tanaka and Wakayama (2015), it is assumed that the flow is inviscid and irrotational inside each fluid layer. The inviscid model inevitably causes a discontinuity of shear stress around the interface. In practice, this drawback would be smeared out, and the analyses presented in this paper should therefore be useful. Figure 1 illustrates the layered system for stable stratification density when $\rho_1 < \rho_2$. Here, (x, y, z) represents the Cartesian coordinate system, where $z = 0$ is a horizontal plane located at the undisturbed interface between the fluid layers and z is measured vertically upwards. The two-fluid system is bounded above and below by rigid surfaces located at $z = h_1$ and $z = -h_2$, respectively. The governing equations for each layer, kinematic boundary conditions, and kinematic and dynamic interface conditions are

$$\nabla^2\phi_1 = 0, \quad \zeta(x,y,t) < z < h_1, \tag{3}$$

$$\nabla^2\phi_2 = 0, \quad -h_2 < z < \zeta(x,y,t), \tag{4}$$

$$\frac{\partial\phi_1}{\partial z} = 0 \quad \text{at } z = h_1, \tag{5}$$

$$\frac{\partial\phi_2}{\partial z} = 0 \quad \text{at } z = -h_2, \tag{6}$$

$$\frac{\partial\zeta}{\partial t} + \nabla\phi_1\cdot\nabla\zeta - \frac{\partial\phi_1}{\partial z} = 0 \quad \text{at } z = \zeta(x,y,t), \tag{7}$$

$$\frac{\partial\zeta}{\partial t} + \nabla\phi_2\cdot\nabla\zeta - \frac{\partial\phi_2}{\partial z} = 0 \quad \text{at } z = \zeta(x,y,t), \tag{8}$$

$$\rho_1\left(\frac{\partial\phi_1}{\partial t} + g\zeta + \frac{1}{2}|\nabla\phi_1|^2\right) - \rho_2\left(\frac{\partial\phi_2}{\partial t} + g\zeta + \frac{1}{2}|\nabla\phi_2|^2\right) = 0 \quad \text{at } z = \zeta(x,y,t), \tag{9}$$

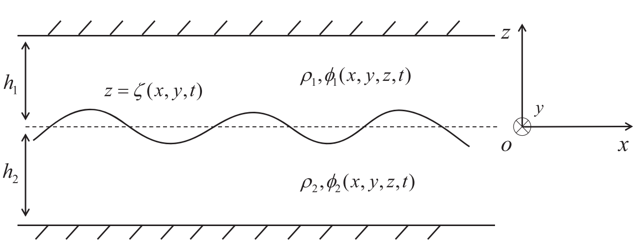

FIG. 1. The physical sketch of the two-fluid system with related notations.

where $\phi_1(x, y, z, t)$ and $\phi_2(x, y, z, t)$ denote the velocity potentials of the upper and lower fluid layers, respectively, $\zeta(x, y, t)$ is the interfacial wave elevation, g is the acceleration due to gravity, t is time, and $\nabla = \boldsymbol{i}\frac{\partial}{\partial x} + \boldsymbol{j}\frac{\partial}{\partial y} + \boldsymbol{k}\frac{\partial}{\partial z}$ is the gradient operator. For constant values of layer density,

$$\rho_1 = \rho_2\Delta, \quad 0 < \Delta < 1, \tag{10}$$

where Δ is the density ratio. Consider a steady-state interfacial wave system with two primary periodic progressive waves. Let $\boldsymbol{k}_i$ denote the wave vector, σ_i denote the actual angular frequency, and β_i denote the initial phase of the ith primary component. As amplitudes of all components in the steady-state interfacial wave system are time-independent, we introduce the following transformation to search for steady-state solutions:

$$\xi_i = \boldsymbol{k}_i \cdot \boldsymbol{r} - \sigma_i t + \beta_i, \quad i = 1, 2, \tag{11}$$

where $\boldsymbol{r} = \boldsymbol{i}x + \boldsymbol{j}y$, and define

$$\begin{gathered}\varphi_1(\xi_1, \xi_2, z) = \phi_1(x, y, z, t), \quad \varphi_2(\xi_1, \xi_2, z) = \phi_2(x, y, z, t), \\ \eta(\xi_1, \xi_2) = \zeta(x, y, t)\end{gathered} \tag{12}$$

in the new coordinate system (ξ_1, ξ_2, z). The original initial/boundary-value problem (3)–(9) in the coordinate system (x, y, z, t) is then transformed into a boundary-value problem in the coordinate system (ξ_1, ξ_2, z). Steady-state solutions can be more easily obtained from the boundary-value problem in the coordinate system (ξ_1, ξ_2, z), and therefore, the two coordinates (ξ_1, ξ_2) play an important role in the rest of the analysis. The governing equations in the coordinate system (ξ_1, ξ_2, z) read

$$\widehat{\nabla}^2\varphi_1 = 0, \quad \eta(\xi_1, \xi_2) < z < h_1, \tag{13}$$

$$\widehat{\nabla}^2\varphi_2 = 0, \quad -h_2 < z < \eta(\xi_1, \xi_2), \tag{14}$$

with three (two kinematic and one dynamic) boundary conditions at the unknown interface $z = \eta(\xi_1, \xi_2)$ (see Appendix A for a detailed derivation),

$$\begin{aligned}\mathcal{N}_1[\varphi_1, \varphi_2] = &\sum_{i=1}^{2}\sum_{j=1}^{2}\sigma_i\sigma_j\frac{\partial^2\varphi_2}{\partial\xi_i\partial\xi_j} + g(1-\Delta)\frac{\partial\varphi_2}{\partial z} \\ &- \Delta\sum_{i=1}^{2}\sum_{j=1}^{2}\sigma_i\sigma_j\frac{\partial^2\varphi_1}{\partial\xi_i\partial\xi_j} + \widehat{\nabla}\varphi_2\cdot\widehat{\nabla}f_2 \\ &- 2\sum_{i=1}^{2}\sigma_i\frac{\partial f_2}{\partial\xi_i} + \Delta\left(\sum_{i=1}^{2}\sigma_i\frac{\partial f_1}{\partial\xi_i}h_{21} - \widehat{\nabla}\varphi_2\cdot\widehat{\nabla}f_1\right) = 0,\end{aligned} \tag{15}$$

$$\begin{aligned}\mathcal{N}_2[\varphi_1, \varphi_2] = &\, g(1-\Delta)\frac{\partial(\varphi_2 - \varphi_1)}{\partial z} + \widehat{\nabla}(\varphi_2 - \varphi_1)\cdot\widehat{\nabla}f_2 - h_{12} \\ &- \sum_{i=1}^{2}\sigma_i\frac{\partial f_2}{\partial\xi_i} - \Delta\left[\sum_{i=1}^{2}\sigma_i\frac{\partial f_1}{\partial\xi_i} + h_{21} + \widehat{\nabla}(\varphi_2 - \varphi_1)\cdot\widehat{\nabla}f_1\right] = 0,\end{aligned} \tag{16}$$

$$\begin{aligned}\mathcal{N}_3[\varphi_1, \varphi_2, \eta] = \eta - &\frac{1}{g(1-\Delta)}\left[\sum_{i=1}^{2}\sigma_i\frac{\partial\varphi_2}{\partial\xi_i} - f_2\right. \\ &\left. - \Delta\left(\sum_{i=1}^{2}\sigma_i\frac{\partial\varphi_1}{\partial\xi_i} - f_1\right)\right] = 0,\end{aligned} \tag{17}$$

and two boundary conditions at the upper and lower rigid surfaces,

$$\frac{\partial\varphi_1}{\partial z} = 0 \quad \text{at } z = h_1, \tag{18}$$

$$\frac{\partial\varphi_2}{\partial z} = 0 \quad \text{at } z = -h_2, \tag{19}$$

where $\mathcal{N}_1$, $\mathcal{N}_2$, and $\mathcal{N}_3$ are nonlinear differential operators and

$$\widehat{\nabla} = \boldsymbol{k}_1\frac{\partial}{\partial\xi_1} + \boldsymbol{k}_2\frac{\partial}{\partial\xi_2} + \boldsymbol{k}\frac{\partial}{\partial z}, \quad f_i = \frac{1}{2}\left|\widehat{\nabla}\varphi_i\right|^2, \quad i = 1, 2, \tag{20}$$

$$h_{ij} = -\sigma_1\widehat{\nabla}\varphi_i\cdot\widehat{\nabla}\left(\frac{\partial\varphi_j}{\partial\xi_1}\right) - \sigma_2\widehat{\nabla}\varphi_i\cdot\widehat{\nabla}\left(\frac{\partial\varphi_j}{\partial\xi_2}\right), \quad i, j = 1, 2. \tag{21}$$

The interfacial wave elevation η and velocity potentials in the upper and lower fluid layers φ_i of the steady-state interfacial wave system can be expressed in the following form:

$$\eta(\xi_1, \xi_2) = \sum_{i=-\infty}^{+\infty}\sum_{j=-\infty}^{+\infty}C_{i,j}^{\eta}\cos(i\xi_1 + j\xi_2), \tag{22}$$

$$\varphi_1(\xi_1, \xi_2, z) = \sum_{i=-\infty}^{+\infty}\sum_{j=-\infty}^{+\infty}C_{i,j}^{\varphi_1}\psi_{i,j}^1(\xi_1, \xi_2, z), \tag{23}$$

$$\varphi_2(\xi_1, \xi_2, z) = \sum_{i=-\infty}^{+\infty}\sum_{j=-\infty}^{+\infty}C_{i,j}^{\varphi_2}\psi_{i,j}^2(\xi_1, \xi_2, z), \tag{24}$$

where

$$\psi_{i,j}^1(\xi_1, \xi_2, z) = \cosh[|i\boldsymbol{k}_1 + j\boldsymbol{k}_2|(z - h_1)]\sin(i\xi_1 + j\xi_2), \tag{25}$$

$$\psi_{i,j}^2(\xi_1, \xi_2, z) = \cosh[|i\boldsymbol{k}_1 + j\boldsymbol{k}_2|(z + h_2)]\sin(i\xi_1 + j\xi_2). \tag{26}$$

The values of $\boldsymbol{k}_i$, σ_i, and h_i with $i = 1, 2$ are given in each case to obtain the unknown constants $C_{i,j}^{\eta}$, $C_{i,j}^{\varphi_1}$, and $C_{i,j}^{\varphi_2}$. Equations (13), (14), (18), and (19) are automatically satisfied by the form of η, φ_i given by (22)–(24), and so the unknown constants are obtained by solving the three boundary conditions (15)–(17) at the internal interface $z = \eta(\xi_1, \xi_2)$.

B. Approach based on the HAM

The general idea behind the homotopy analysis method (HAM) is to construct a kind of continuous deformation between the given solution (called initial guess) and the solution of the nonlinear differential equations to be solved. A detailed introduction of the HAM can be found in Liao (2003; 2011a) and Vajravelu and Van Gorder (2012). The basic concept and important details of the HAM are described below.

Given that the expressions for φ_1 (23) and φ_2 (24) automatically satisfy the governing equations (13) and (14) and the top and bottom boundary conditions [(18) and (19)], it is sufficient solely to consider the interface conditions (15) and (17). We set $q \in [0, 1]$ as an embedding homotopy parameter, $c_0 \neq 0$ as a convergence-control parameter, $\mathcal{L}_1$ and $\mathcal{L}_2$ as the auxiliary linear operators, $\eta_0 = 0$ as the initial approximation of interfacial wave elevation η, and $\varphi_{0,1}(\xi_1, \xi_2, z)$ and $\varphi_{0,2}(\xi_1, \xi_2, z)$ as the initial approximations of the potential functions φ_1 and φ_2. Then, based on the interface conditions (15)–(17), we construct the following parameterized family of equations (called the zeroth-order deformation equations):

$$(1-q)\mathcal{L}_1[\check{\varphi}_1-\varphi_{0,1},\check{\varphi}_2-\varphi_{0,2}]=qc_0\mathcal{N}_1[\check{\varphi}_1,\check{\varphi}_2]\quad \text{at } z=\check{\eta}, \tag{27}$$

$$(1-q)\mathcal{L}_2[\check{\varphi}_1-\varphi_{0,1},\check{\varphi}_2-\varphi_{0,2}]=qc_0\mathcal{N}_2[\check{\varphi}_1,\check{\varphi}_2]\quad \text{at } z=\check{\eta}, \tag{28}$$

$$(1-q)\check{\eta}=qc_0\mathcal{N}_3[\check{\varphi}_1,\check{\varphi}_2,\check{\eta}]\quad \text{at } z=\check{\eta}, \tag{29}$$

where

$$\begin{aligned}\check{\varphi}_i(\xi_1,\xi_2,z;q)&=\sum_{m=0}^{+\infty}\varphi_{m,i}q^m,\\ \varphi_{m,i}(\xi_1,\xi_2,z)&=\frac{1}{m!}\frac{\partial^m\check{\varphi}_i}{\partial q^m}\bigg|_{q=0},\quad i=1,2,\end{aligned} \tag{30}$$

$$\check{\eta}(\xi_1,\xi_2;q)=\sum_{m=1}^{+\infty}\eta_m q^m,\quad \eta_m(\xi_1,\xi_2)=\frac{1}{m!}\frac{\partial^m\check{\eta}}{\partial q^m}\bigg|_{q=0}. \tag{31}$$

Considering the auxiliary linear operators $\mathcal{L}_1$ and $\mathcal{L}_2$ that have the property $\mathcal{L}_1[0,0]=\mathcal{L}_2[0,0]=0$, we obtain the following relationships when $q=0$:

$$\check{\varphi}_i(\xi_1,\xi_2,z;0)=\varphi_{0,i},\quad i=1,2,\quad \check{\eta}(\xi_1,\xi_2;0)=0. \tag{32}$$

When $q=1$, Eqs. (27)–(29) are equivalent to the original equations (15)–(17). Thus,

$$\check{\varphi}_i(\xi_1,\xi_2,z;1)=\varphi_i,\quad i=1,2,\quad \check{\eta}(\xi_1,\xi_2;1)=\eta. \tag{33}$$

Hence, Eqs. (27)–(29) define the following three homotopies:

$$\check{\varphi}_1:=\varphi_{0,1}\sim\varphi_1,\quad \check{\varphi}_2:=\varphi_{0,2}\sim\varphi_2,\quad \check{\eta}:=0\sim\eta,\quad \text{when } q:=0\sim 1. \tag{34}$$

Letting $q=1$, the solutions for the interfacial wave elevation η and velocity potentials in the upper and lower fluid layers φ_i are approximated by

$$\varphi_i(\xi_1,\xi_2,z)=\check{\varphi}_i(\xi_1,\xi_2,z;1)=\sum_{m=0}^{+\infty}\varphi_{m,i}(\xi_1,\xi_2,z),\quad i=1,2, \tag{35}$$

$$\eta(\xi_1,\xi_2)=\check{\eta}(\xi_1,\xi_2;1)=\sum_{m=1}^{+\infty}\eta_m(\xi_1,\xi_2). \tag{36}$$

The sum index of the interfacial wave elevation η starts from $m=1$ as the initial guess $\eta_0=0$.

1. Solution procedure

The unknowns $\varphi_{m,i}$ and η_m are governed by the following high-order deformation equations:

$$\overline{\mathcal{L}}_i[\varphi_{m,1},\varphi_{m,2}]=c_0\Delta^{\varphi}_{m-1,i}-\overline{S}_{m,i}+\chi_m S_{m-1,i},\quad i=1,2, \tag{37}$$

$$\eta_m=c_0\Delta^{\eta}_{m-1}+\chi_m\eta_{m-1}, \tag{38}$$

where $\chi_1=0$ and $\chi_m=1$ for $m\geq 2$, and $\overline{\mathcal{L}}_i=\mathcal{L}_i|_{z=0}$ are auxiliary linear operators.

Up to the mth-order of approximation, all terms $\Delta^{\varphi}_{m-1,i}$, $\overline{S}_{m,i}$, $S_{m-1,i}$, and Δ^{η}_{m-1} on the right-hand side of the high-order deformation equations (37) and (38) are already predetermined by $\varphi_{n,i}$ and η_n, with $n=0, 1, 2, \ldots, m-1$ and $m\geq 1$. The detailed expressions for $\Delta^{\varphi}_{m-1,i}$, $\overline{S}_{m,i}$, $S_{m-1,I}$, and Δ^{η}_{m-1} are given in Appendix B and Sec. II B 2. Note that η_m could be obtained directly from (38); meanwhile, the solution process for $\varphi_{m,i}$ is more complicated.

When resonance conditions are nearly satisfied, proper auxiliary linear operators $\mathcal{L}_i$ must be chosen to remove the small divisors associated with the near-resonant components in $\varphi_{m,i}$. Otherwise, no convergent series solutions could be obtained for steady-state wave groups. This is why the perturbation method breaks down for steady-state wave groups when the resonance conditions are satisfied (Madsen and Fuhrman, 2012). Unlike the traditional perturbation method, the HAM does not depend on small physical parameters and instead provides freedom in the choices of auxiliary linear operator and initial guess. Convergent series solutions can therefore be obtained in the HAM framework for steady-state resonant wave groups.

2. Choice of auxiliary linear operators

Consider an interfacial wave system with L nearly resonant components ($\boldsymbol{k}_{0,1}$, $\boldsymbol{k}_{0,2}$, …, $\boldsymbol{k}_{0,L}$) and two primary ones ($\boldsymbol{k}_1$, $\boldsymbol{k}_2$). The resonance criteria are

$$i_l\boldsymbol{k}_1+j_l\boldsymbol{k}_2=\boldsymbol{k}_{0,l},\quad i_l\omega_1+j_l\omega_2=\omega_{0,l}+d\omega_{0,l},\quad l=1,2,\ldots,L, \tag{39}$$

where

$$\omega_i=\omega(k_i)=\sqrt{\frac{gk_i(1-\Delta)\tanh(k_ih_1)\tanh(k_ih_2)}{\tanh(k_ih_1)+\Delta\tanh(k_ih_2)}} \tag{40}$$

is the linear angular frequency with the associated wave number $k_i=|\boldsymbol{k}_i|$. Here, $d\omega_{0,l}$ is a small real number that represents the angular frequency mismatch of the lth resonant component.

For multiple resonances such as given by (39), the following auxiliary linear operators can be used to eliminate the small divisor caused by each nearly resonant component:

$$\begin{aligned}\mathcal{L}_1[\varphi_1,\varphi_2]&=\omega_1^2\frac{\partial^2\varphi_2}{\partial\xi_1^2}+\mu\omega_1\omega_2\frac{\partial^2\varphi_2}{\partial\xi_1\partial\xi_2}\\&\quad+\omega_2^2\frac{\partial^2\varphi_2}{\partial\xi_2^2}+g(1-\Delta)\frac{\partial\varphi_2}{\partial z}\\&\quad-\Delta\left(\omega_1^2\frac{\partial^2\varphi_1}{\partial\xi_1^2}+\mu\omega_1\omega_2\frac{\partial^2\varphi_1}{\partial\xi_1\partial\xi_2}+\omega_2^2\frac{\partial^2\varphi_1}{\partial\xi_2^2}\right),\end{aligned} \tag{41}$$

$$\mathcal{L}_2[\varphi_1,\varphi_2]=g(1-\Delta)\left(\frac{\partial\varphi_2}{\partial z}-\frac{\partial\varphi_1}{\partial z}\right), \tag{42}$$

where

$$\mu(i,j)=\begin{cases}\frac{\omega^2(k_{i,j})-(i^2\omega_1^2+j^2\omega_2^2)}{ij\omega_1\omega_2}, & i=i_l, j=j_l\\ 2, & \text{else}\end{cases} \tag{43}$$

is a piecewise parameter depending on i and j in φ_i [(23) and (24)] and $k_{i,j}=|i\boldsymbol{k}_1+j\boldsymbol{k}_2|$. This piecewise parameter is the key that eliminates the small divisors caused by all nearly resonant components and makes the HAM work. The auxiliary linear operators [(41) and

(42)] are chosen based on the linear operators in boundary conditions [(15) and (16)]. The expressions of $S_{m,i}$ and $\overline{S}_{m,i}$ can then be defined as

$$S_{m,1} = \omega_1^2\beta_{2,0,2}^{m,0} + \mu\omega_1\omega_2\beta_{1,1,2}^{m,0} + \omega_2^2\beta_{0,2,2}^{m,0} + g(1-\Delta)\gamma_{0,0,2}^{m,0} - \Delta\left(\omega_1^2\beta_{2,0,1}^{m,0} + \mu\omega_1\omega_2\beta_{1,1,1}^{m,0} + \omega_2^2\beta_{0,2,1}^{m,0}\right) + \overline{S}_{m,1}, \tag{44}$$

$$\overline{S}_{m,1} = \sum_{n=1}^{m-1}\Big[\omega_1^2\beta_{2,0,2}^{m-n,n} + \mu\omega_1\omega_2\beta_{1,1,2}^{m-n,n} + \omega_2^2\beta_{0,2,2}^{m-n,n} + g(1-\Delta)\gamma_{0,0,2}^{m-n,n} - \Delta\left(\omega_1^2\beta_{2,0,1}^{m-n,n} + \mu\omega_1\omega_2\beta_{1,1,1}^{m-n,n} + \omega_2^2\beta_{0,2,1}^{m-n,n}\right)\Big], \tag{45}$$

$$\overline{S}_{m,2} = \sum_{n=1}^{m-1}\Big[g(1-\Delta)\left(\gamma_{0,0,2}^{m-n,n} - \gamma_{0,0,1}^{m-n,n}\right)\Big], \tag{46}$$

$$S_{m,2} = g(1-\Delta)\left(\gamma_{0,0,2}^{m,0} - \gamma_{0,0,1}^{m,0}\right) + \overline{S}_{m,2}. \tag{47}$$

The detailed expressions of $\beta_{i,j,k}^{n,m}$ and $\gamma_{i,j,k}^{n,m}$ are shown in Appendix B. Define the general form of $\varphi_{m,1}$ and $\varphi_{m,2}$ as

$$\varphi_{m,1} = \sum_{i,j} C_{i,j}^{\varphi_1,m}\psi_{i,j}^1, \quad \varphi_{m,2} = \sum_{i,j} C_{i,j}^{\varphi_2,m}\psi_{i,j}^2. \tag{48}$$

Then, the mth-order deformation equation (37) can be simplified as

$$\overline{\mathcal{L}}_1\left[\sum_{i,j} C_{i,j}^{\varphi_1,m}\psi_{i,j}^1, \sum_{i,j} C_{i,j}^{\varphi_2,m}\psi_{i,j}^2\right] = \sum_{i,j} R_{i,j}^{1,m}\sin(i\xi_1 + j\xi_2), \tag{49}$$

$$\overline{\mathcal{L}}_2\left[\sum_{i,j} C_{i,j}^{\varphi_1,m}\psi_{i,j}^1, \sum_{i,j} C_{i,j}^{\varphi_2,m}\psi_{i,j}^2\right] = \sum_{i,j} R_{i,j}^{2,m}\sin(i\xi_1 + j\xi_2), \tag{50}$$

where $C_{i,j}^{\varphi_1,m}$ and $C_{i,j}^{\varphi_2,m}$ are the constants to be determined for given $R_{i,j}^{1,m}$ and $R_{i,j}^{2,m}$. Equating the terms of both sides of Eqs. (49) and (50), we obtain the following two linear algebraic equations:

$$\Delta(i^2\omega_1^2 + \mu ij\omega_1\omega_2 + j^2\omega_2^2)\cosh(k_{i,j}h_1)C_{i,j}^{\varphi_1,m} + \big[g(1-\Delta)k_{i,j}\sinh(k_{i,j}h_2) - (i^2\omega_1^2 + \mu ij\omega_1\omega_2 + j^2\omega_2^2)\cosh(k_{i,j}h_2)\big]C_{i,j}^{\varphi_2,m} = R_{i,j}^{1,m}, \tag{51}$$

$$g(1-\Delta)k_{i,j}\Big[\sinh(k_{i,j}h_1)C_{i,j}^{\varphi_1,m} + \sinh(k_{i,j}h_2)C_{i,j}^{\varphi_2,m}\Big] = R_{i,j}^{2,m}. \tag{52}$$

The solutions for $C_{i,j}^{\varphi_1,m}$ and $C_{i,j}^{\varphi_2,m}$ are given by

$$C_{i,j}^{\varphi_1,m} = \frac{R_{i,j}^{2,m}}{g(1-\Delta)k_{i,j}\sinh(k_{i,j}h_1)} - \frac{\sinh(k_{i,j}h_2)}{\sinh(k_{i,j}h_1)}C_{i,j}^{\varphi_2,m}, \tag{53}$$

$$C_{i,j}^{\varphi_2,m} = \frac{A_{i,j}}{\lambda_{i,j}}\left(R_{i,j}^{1,m} - B_{i,j}R_{i,j}^{2,m}\right), \tag{54}$$

respectively, where

$$A_{i,j} = \frac{\tanh(k_{i,j}h_1)/\cosh(k_{i,j}h_2)}{\tanh(k_{i,j}h_1) + \Delta\tanh(k_{i,j}h_2)}, \tag{55}$$

$$B_{i,j} = \frac{\Delta(i^2\omega_1^2 + \mu ij\omega_1\omega_2 + j^2\omega_2^2)}{g(1-\Delta)k_{i,j}\tanh(k_{i,j}h_1)}, \tag{56}$$

$$\lambda_{i,j} = \omega^2(k_{i,j}) - (i^2\omega_1^2 + \mu ij\omega_1\omega_2 + j^2\omega_2^2). \tag{57}$$

For a non-resonant component $\cos(i\xi_1 + j\xi_2)$, $\mu(i,j) = 2$ and $\lambda_{i,j} = \omega^2(k_{i,j}) - (i\omega_1 + j\omega_2)^2$ is a non-small real number. $C_{i,j}^{\varphi_2,m}$ can be obtained directly from (54), and $C_{i,j}^{\varphi_1,m}$ is then computed from (53). For a nearly resonant component $\cos(i_l\xi_1 + j_l\xi_2)$, the value of $\mu(i_l, j_l)$ is determined so that it satisfies $\lambda_{i_l,j_l} = \omega^2(k_{i_l,j_l}) - (i_l^2\omega_1^2 + \mu i_l j_l\omega_1\omega_2 + j_l^2\omega_2^2) = 0$. Small divisors caused by nearly resonant components are changed into singularities associated with exact resonance. Since $\lambda_{i_l,j_l} = 0$ for a nearly resonant component, then $C_{i_l,j_l}^{\varphi_2,m}$ cannot be obtained from (54) directly. To remove the singularity associated with the resonance, we enforce the right-hand side of (54) equal to zero,

$$R_{i_l,j_l}^{1,m} - \frac{\Delta\tanh(k_{i_l,j_l}h_2)}{\tanh(k_{i_l,j_l}h_1) + \Delta\tanh(k_{i_l,j_l}h_2)}R_{i_l,j_l}^{2,m} = 0, \tag{58}$$

from which the value of $C_{i_l,j_l}^{\varphi_2,m-1}$ is determined. Similarly, $C_{i_l,j_l}^{\varphi_2,m}$ is determined from the right-hand side of (54) via

$$R_{i_l,j_l}^{1,m+1} - \frac{\Delta\tanh(k_{i_l,j_l}h_2)}{\tanh(k_{i_l,j_l}h_1) + \Delta\tanh(k_{i_l,j_l}h_2)}R_{i_l,j_l}^{2,m+1} = 0. \tag{59}$$

It should be noted that for the two primary components $\cos(\xi_1)$ and $\cos(\xi_2)$, $\lambda_{1,0} = \lambda_{0,1} = 0$. Therefore, $C_{1,0}^{\varphi_2,m}$ and $C_{0,1}^{\varphi_2,m}$ are determined in a similar way as if the two primary components are resonant ones. Once the value of $C_{i,j}^{\varphi_2,m}$ is obtained, we can compute $C_{i,j}^{\varphi_1,m}$ directly from (53).

3. Choice of initial velocity potentials

Based on the linearized solutions of Eqs. (15)–(17), we choose the following initial guesses:

$$\varphi_{0,1} = -\frac{\sinh(k_1h_2)}{\sinh(k_1h_1)}C_{1,0}^{\varphi_2,0}\psi_{1,0}^1 - \frac{\sinh(k_2h_2)}{\sinh(k_2h_1)}C_{0,1}^{\varphi_2,0}\psi_{0,1}^1 - \sum_{i=1}^{L}\frac{\sinh(k_{i_l,j_l}h_2)}{\sinh(k_{i_l,j_l}h_1)}C_{i_l,j_l}^{\varphi_2,0}\psi_{i_l,j_l}^1, \tag{60}$$

$$\varphi_{0,2} = C_{1,0}^{\varphi_2,0}\psi_{1,0}^2 + C_{0,1}^{\varphi_2,0}\psi_{0,1}^2 + \sum_{l=1}^{L}C_{i_l,j_l}^{\varphi_2,0}\psi_{i_l,j_l}^2 \tag{61}$$

for velocity potentials and $\eta_0 = 0$ for the interfacial wave elevation. Here, the relationship between coefficients of $\psi_{i,j}^1$ and $\psi_{i,j}^2$ is derived directly from (53). When $m = 1$, Eq. (58) reduces to nonlinear algebraic equations from which multiple solutions can be obtained for $C_{i,j}^{\varphi_2,0}$. When $m > 1$, Eq. (58) reduces to linear algebraic equations for $C_{i,j}^{\varphi_2,m-1}$. For weakly nonlinear waves, one resonant component in the initial guesses (60) and (61) ($L = 1$) is considered in order to obtain convergent steady-state solutions. As the nonlinearity (wave steepness) increases, the wave energy increases and is more dispersed. Other components may join the resonance, and so the number of resonant components (L) in the initial guess increases, too. A detailed example is given in Sec. III C.

In the framework of the HAM, the proper auxiliary linear operator and initial guess are chosen to remove the small divisors associated with near resonance. Convergent series solutions could then be obtained successfully by symbolic arithmetic software such as Mathematica. Compared with the solution procedure of multiple steady-state resonances for surface waves (Liu *et al.*, 2018; Liu and Xie, 2019), the solution procedure for interfacial waves is more complicated. One more unknown velocity potential is considered in the kinematic and dynamic interface conditions. Besides, the velocity potentials in the upper and lower fluid layers are coupled, so they have to be solved simultaneously. The CUP time required for convergent series solutions of steady-state resonant interfacial waves increases dramatically when either the order of approximation or the number of near-resonant components in the initial guess increases. To accelerate the convergence rate of series solutions provided by the HAM, we combine the HAM-based analytical approach and Galerkin method-based numerical approach. Once convergent series solutions of steady-state resonant interfacial waves have been found by HAM, the Galerkin method is used to obtain accurate steady-state solutions as the nonlinearity or density ratio changes.

C. Approach based on Galerkin's method

Based on the work of Okamura (2010) and Liu and Xie (2019), we express the interfacial wave elevation η and velocity potentials φ_i as

$$\eta(\xi_1,\xi_2) = \sum_{i=1}^{N}\sum_{j=-N}^{N} C_{i,j}^{\eta}\cos(i\xi_1 + j\xi_2) + \sum_{j=0}^{N} C_{0,j}^{\eta}\cos(j\xi_2), \tag{62}$$

$$\begin{aligned}\varphi_1(\xi_1,\xi_2,z) = &\sum_{i=1}^{N}\sum_{j=-N}^{N} C_{i,j}^{\varphi_1}\psi_{i,j}^{1}(\xi_1,\xi_2,z)\\ &+\sum_{j=1}^{N} C_{0,j}^{\varphi_1}\psi_{0,j}^{1}(\xi_1,\xi_2,z),\end{aligned} \tag{63}$$

$$\begin{aligned}\varphi_2(\xi_1,\xi_2,z) = &\sum_{i=1}^{N}\sum_{j=-N}^{N} C_{i,j}^{\varphi_2}\psi_{i,j}^{2}(\xi_1,\xi_2,z)\\ &+\sum_{j=1}^{N} C_{0,j}^{\varphi_2}\psi_{0,j}^{2}(\xi_1,\xi_2,z)\end{aligned} \tag{64}$$

with $6N(N+1)+1$ unknown coefficients ($C_{i,j}^{\eta}$, $C_{i,j}^{\varphi_1}$, and $C_{i,j}^{\varphi_2}$) to be determined.

After substituting (63) and (64) into (17), the discrete interface profile,

$$z = \eta(\xi_1,\xi_2) = \eta\Big(\frac{2\pi(i-1)}{M}, \frac{2\pi(j-1)}{M}\Big), \quad i,j = 1,2,\ldots,M, \tag{65}$$

can be evaluated numerically by Newton's method for M^2 discrete points. Then, substituting (65) into (15) and (16), we obtain

$$P_{r,s} = \int_0^{2\pi}\int_0^{2\pi} \mathcal{N}_1[\varphi_1,\varphi_2]\sin(r\xi_1 + s\xi_2)d\xi_1 d\xi_2 = 0, \quad \text{at } z = \eta(\xi_1,\xi_2), \tag{66}$$

$$Q_{r,s} = \int_0^{2\pi}\int_0^{2\pi} \mathcal{N}_2[\varphi_1,\varphi_2]\sin(r\xi_1 + s\xi_2)d\xi_1 d\xi_2 = 0, \quad \text{at } z = \eta(\xi_1,\xi_2), \tag{67}$$

which are calculated using M-point Fourier transforms. For $M > 2N+1$, $4N(N+1)$ independent equations can be obtained from (66) and (67) for $1 \le r \le N$, $-N \le s \le N$, and $1 \le s \le N$ with $r = 0$. The number of unknown coefficients $C_{i,j}^{\varphi_1}$ and $C_{i,j}^{\varphi_2}$ in the velocity potentials φ_1 and φ_2, $4N(N+1)$ equals the number of equations in (66) and (67). Hence, the values of $C_{i,j}^{\varphi_1}$ and $C_{i,j}^{\varphi_2}$ can be computed by Newton's method. Finally, we substitute (63) and (64) into (17) and obtain

$$R_{r,s} = \int_0^{2\pi}\int_0^{2\pi} \mathcal{N}_3[\varphi_1,\varphi_2,\eta]\cos(r\xi_1 + s\xi_2)d\xi_1 d\xi_2 = 0, \quad \text{at } z = \eta(\xi_1,\xi_2), \tag{68}$$

which is evaluated by means of an M-point Fourier transform. For $M > 2N+1$, $2N(N+1)+1$ independent equations from (68) are obtained for $1 \le r \le N$, $-N \le s \le N$, and $0 \le s \le N$ with $r = 0$. The number of unknown coefficients $C_{i,j}^{\eta}$ in the interfacial wave elevation η, $2N(N+1)$, equals the number of equations in (68), and so $C_{i,j}^{\eta}$ is also determined using Newton's method. When applying Galerkin's method, the initial solution is provided by the HAM, and the iterations terminated once the maximum absolute difference between the unknown coefficients before and after an iteration reduces below 10^{-9}. Appendix C lists the full details of the formulas used to evaluate the coefficients in the Jacobian matrices.

We define the dimensionless angular frequency $\epsilon = \sigma_1/\omega_1 = \sigma_2/\omega_2$ and the wave steepness

$$H_s = k_2\frac{max[\eta(\xi_1,\xi_2)] - min[\eta(\xi_1,\xi_2)]}{2}, \quad \xi_1,\xi_2 \in [0,2\pi]. \tag{69}$$

Here, the wave number of the second primary component k_2 is used because its value is fixed in different cases. Table I lists the

TABLE I. Dimensionless amplitude of the dominant component $|C_{4,-3}^{\eta}|k_{4,-3}$ and wave steepness H_s in the form $(|C_{4,-3}^{\eta}|k_{4,-3}, H_s)$ of one solution for various values of N and M when $\Delta = 0.996$, $h_1/\lambda_2 = 0.5$, $h_2/\lambda_2 = 2$, $\alpha = \pi/36$, $k_2/k_1 = 0.895\,815$, and $\epsilon = 1.014$. α is the angle between the wave vectors of the two primary components, and $\lambda_2 = 2\pi/k_2$. "…" means divergent solutions.

$N\backslash M$	69	84	99
25	(0.114 08, 0.265 75)	(0.114 08, 0.265 76)	(0.114 08, 0.265 76)
30	(0.112 20, 0.265 91)	(0.113 66, 0.265 43)	(0.113 66, 0.265 43)
35	…	(0.113 76, 0.265 35)	(0.113 75, 0.265 36)

dimensionless amplitude of the dominant component, $|C^{\eta}_{4,-3}|k_{4,-3}$ (only in this case), and the wave steepness, H_s, for different values of N and M when $\epsilon = 1.014$. It can be seen that the values of $|C^{\eta}_{4,-3}|k_{4,-3}$ and H_s remain unchanged for $M \geq 84$. The values of $|C^{\eta}_{4,-3}|k_{4,-3}$ and H_s converge as N increases from 25 to 35. Convergent solutions up to four significant figures are obtained for this case where $N = 35$ and $M = 99$. In the other cases considered, convergence is up to four significant figures.

III. RESULTS AND ANALYSIS

A. Linear resonance analysis

We first examine linear resonance in a duct. The geometric configuration and physical properties of the fluid layers are based on the following parameters for northeast of the South China Sea at (21°N, 118.5°E) (Fan *et al.*, 2013):

$$\Delta = 0.996, \quad \frac{h_1}{\lambda_2} = 0.5, \quad \frac{h_2}{\lambda_2} = 2, \quad \alpha = \frac{\pi}{36}, \tag{70}$$

where α is the angle between the wave vectors of the two primary components $\boldsymbol{k}_1$ and $\boldsymbol{k}_2$, $\lambda_2 = 2\pi/k_2 = 1$ km is the wavelength of the second primary component (close to real internal waves in the ocean), h_1 is the depth of the upper fluid layer, and h_2 is the depth of the lower layer. We define the relative angular frequency mismatch as

$$\nu(m_l, n_l) = \frac{|d\omega_{0,l}|}{\omega_1}. \tag{71}$$

Figure 2 shows the resonance curves of the second primary component $\boldsymbol{k}_2$ for the given wave vector $\boldsymbol{k}_1$ of the first primary component. Here, the resonance condition (39) is satisfied for any possible combination of the two primary components. It can be seen that

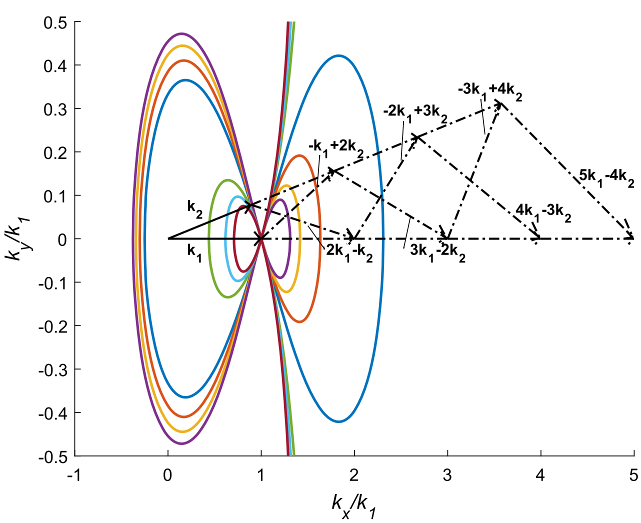

FIG. 2. The curves represent the location of the wave vector $\boldsymbol{k}_2$ (the second primary component) satisfying the resonance condition (39), once the wave vector $\boldsymbol{k}_1$ (the first primary component) is given in the case of (70). The resonance curves remain quite close to each other, which suggests that other components such as $2\boldsymbol{k}_1 - \boldsymbol{k}_2$ and $-\boldsymbol{k}_1 + 2\boldsymbol{k}_2$ may appear in the steady-state wave field while the second primary component moves along the resonance curves.

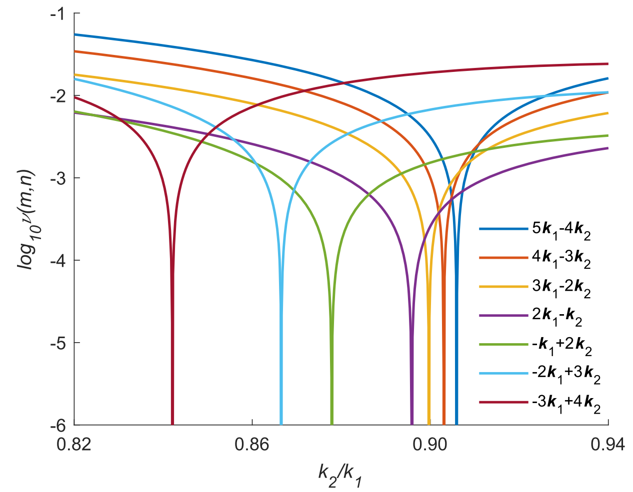

FIG. 3. Relative angular frequency mismatch $\log_{10} \nu(m, n)$ vs wave number ratio k_2/k_1 in the case of (70).

the resonance curves stay close to each other for any possible $\boldsymbol{k}_2$. The other components such as $2\boldsymbol{k}_1 - \boldsymbol{k}_2$ and $-\boldsymbol{k}_1 + 2\boldsymbol{k}_2$ may appear in the steady-state wave field due to resonant interactions.

Taking several possible nearly resonant components as an example, Fig. 3 displays the dependence of relative angular frequency mismatch $\nu(m_l, n_l)$ on the wave number ratio k_2/k_1. It can be seen that resonance occurs when k_2/k_1 is in the range (0.84, 0.91). Here, $k_2/k_1 = 0.895\,815$ is chosen so that the component $(2, -1)$ corresponds to an exactly resonant component. Table II lists the six resonant components with the smallest relative angular frequency mismatches $\log_{10} \nu(m_l, n_l)$. As the nonlinearity increases, these resonant components with small relative angular frequency mismatches may serve as possible candidates for inclusion in the initial guesses (60) and (61).

B. Weakly nonlinear waves with single exactly resonant quartet

Next, we consider weakly nonlinear interfacial wave systems for the case $\epsilon = 1.0002$ together with the parameters in (70). We consider the exactly resonant component $(2, -1)$ and two primary ones in the initial guesses (60) and (61). We define $L = 1$ in (39) and modify the auxiliary linear operator (41) accordingly. For $m = 1$, the nonlinear algebraic equations (58) governing $C^{\varphi_2,0}_{1,0}$, $C^{\varphi_2,0}_{0,1}$ and $C^{\varphi_2,0}_{2,-1}$ have three groups of solutions, listed in Table V in Appendix D, which we call S1, S2, and S3, respectively. The three

TABLE II. Six near-resonant components with the smallest relative angular frequency mismatches $\log_{10} \nu(m_l, n_l)$ in the case of (70) and $k_2/k_1 = 0.895\,815$ for $|m| \leq 20$ and $|n| \leq 20$.

m_l	n_l	$\log_{10} \nu(m_l, n_l)$	m_l	n_l	$\log_{10} \nu(m_l, n_l)$
3	−2	−3.16	5	−4	−2.27
−1	2	−2.90	−2	3	−2.22
4	−3	−2.61	6	−5	−2.01

TABLE III. Wave energy distributions and wave steepness H_s of weakly nonlinear steady-state resonant interfacial waves in the case of (70) with $\epsilon = 1.0002$.

Group	$\frac{(C^{\eta}_{1,0})^2}{\Pi}$ (%)	$\frac{(C^{\eta}_{0,1})^2}{\Pi}$ (%)	$\frac{(C^{\eta}_{2,-1})^2}{\Pi}$ (%)	$\frac{(C^{\eta}_{3,-2})^2}{\Pi}$ (%)	H_s
S1	40.80	50.07	8.813	0.3176	0.0313
S2	41.25	18.52	39.50	0.6580	0.0361
S3	9.800	11.94	78.19	0.0383	0.0351

groups of solutions imply that three balanced states of wave energy exist for the weakly nonlinear cases considered here. It should be emphasized that the number of weakly nonlinear solutions of interfacial waves with a steady-state quartet depends on the physical parameter considered in (70). Further calculations show that the weakly nonlinear solutions of interfacial waves form a continuum in the parameter space. Therefore, the number of weakly nonlinear solutions changes continuously from 3 to 0 when the physical parameters in (70) change. A similar phenomenon has also been found for weakly nonlinear surface waves by Liu and Liao (2014).

The interfacial wave energy of the whole wave system may be defined approximately as

$$\Pi = \sum_{m=-\infty}^{+\infty} \sum_{n=-\infty}^{+\infty} (C^{\eta}_{m,n})^2. \tag{72}$$

Table III summarizes the energy distributions of the three convergent solutions. For weakly nonlinear waves, the total energy Π is mainly contained by the primary components and the exactly resonant component.

Next, we consider the influence of density ratio on weakly nonlinear resonant waves. For (70) and $\epsilon = 1.0002$, we vary the density ratio Δ from 0 to 1. At the same time, the wave number ratio k_2/k_1 changes with Δ so that the component (2, −1) corresponds to an exactly resonant one. Figure 4 shows the wave amplitude $|C^{\eta}_{i,j} k_{i,j}|$ of three solutions as a function of Δ. It is found that as Δ increases, the amplitude of each component increases continuously, which means that the amplitude of each interfacial wave component tends to increase with density ratio.

We define the average velocity along the interfacial wave profile separating the upper and lower layers as

$$U_i = \frac{\int_0^{2\pi}\int_0^{2\pi} \sqrt{u_i^2 + v_i^2 + w_i^2}\Big|_{z=\eta} d\xi_1 d\xi_2}{4\pi^2 H_s \sqrt{g/k_2}}, \quad i = 1, 2, \tag{73}$$

where $(\boldsymbol{i}u_i, \boldsymbol{j}v_i, \boldsymbol{k}w_i) = \nabla\phi_i$. Figure 5 shows the dependence on Δ of the wave steepness H_s and average velocity U_i of three solutions. For all three solutions, the wave steepness H_s increases, and average velocity U_i decreases with Δ. For interfacial waves with an upper layer of larger density, the wave steepness is higher and the average velocity is smaller than that of corresponding interfacial waves with an upper layer of lower density. Existence of an upper layer boosts wave steepness while reducing the average velocity in weakly nonlinear interfacial wave systems.

C. Multiple nearly resonant waves with increased nonlinearity

For wave components traveling in the same direction, the wave steepness increases with the dimensionless angular frequency ϵ. Hence, in this section, the dimensionless angular frequency ϵ is increased to consider steady-state interfacial waves with multiple near resonances. In the HAM-based analytical approach, additional resonant components (see Table II) are considered in the initial guesses (60) and (61) when ϵ increases from 1.0002 to 1.008. The

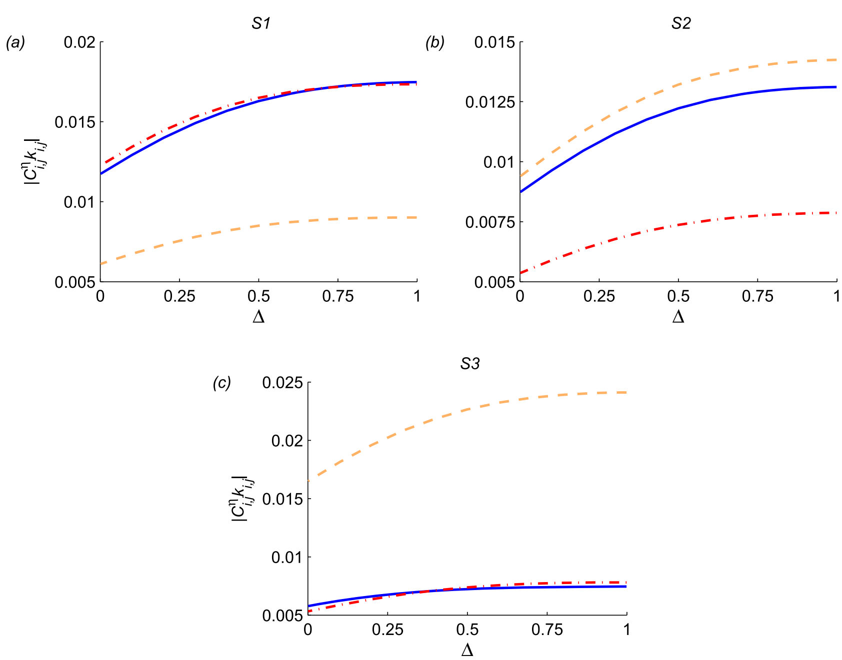

FIG. 4. Wave amplitude $|C^{\eta}_{i,j} k_{i,j}|$ vs Δ with the parameters in (70) when $\epsilon = 1.0002$. Wave number ratio k_2/k_1 changes with Δ so that the component (2, −1) corresponds to the exact resonance. Solid line, $|C^{\eta}_{1,0} k_{1,0}|$; dashed-dotted line, $|C^{\eta}_{0,1} k_{0,1}|$; and dashed line, $|C^{\eta}_{2,-1} k_{2,-1}|$.

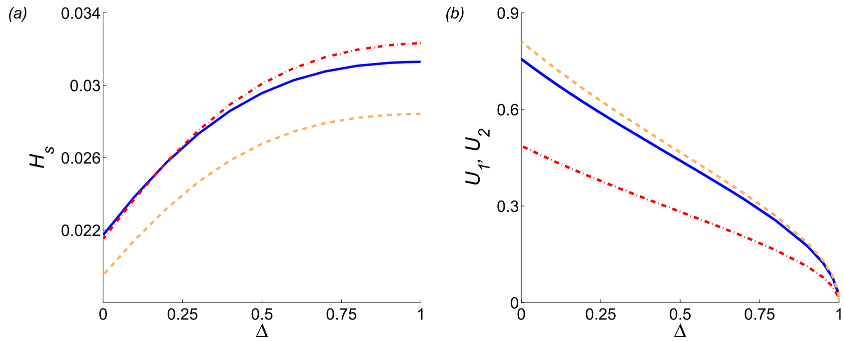

FIG. 5. Wave steepness H_s and average velocity U_i vs Δ with the parameters in (70) when ϵ = 1.0002. Wave number ratio k_2/k_1 changes with Δ so that the component (2, −1) corresponds to the exact resonance. Solid line, S1; dashed-dotted line, S2; and dashed line, S3.

TABLE IV. Energy distributions of steady-state multiple nearly resonant interfacial waves for different values of dimensionless angular frequency ϵ in group S2 in the case of (70). "⋯" means the wave component is small enough to be ignored.

	Dimensionless angular frequency ϵ								
Energy distributions	1.0002	1.002	1.004	1.006	1.008	1.01	1.012	1.014	1.0147
$(C^{\eta}_{1,0})^2/\Pi$ (%)	41.25	19.09	2.640	⋯	1.661	3.598	4.200	3.356	2.883
$(C^{\eta}_{0,1})^2/\Pi$ (%)	18.52	1.615	3.432	7.335	6.908	4.295	1.364	⋯	0.120
$(C^{\eta}_{2,-1})^2/\Pi$ (%)	39.50	42.39	32.81	18.34	7.040	1.217	⋯	0.772	0.815
$(C^{\eta}_{3,-2})^2/\Pi$ (%)	0.658	19.11	34.07	40.88	35.89	24.51	13.92	7.998	8.262
$(C^{\eta}_{-1,2})^2/\Pi$ (%)	⋯	15.00	18.12	9.701	3.668	0.378	0.578	4.188	6.711
$(C^{\eta}_{4,-3})^2/\Pi$ (%)	⋯	2.579	6.953	17.53	29.59	35.47	34.38	31.48	31.24
$(C^{\eta}_{5,-4})^2/\Pi$ (%)	⋯	0.120	⋯	0.822	5.541	13.84	20.75	23.06	19.66
$(C^{\eta}_{-2,3})^2/\Pi$ (%)	⋯	⋯	1.364	3.458	7.255	13.48	19.64	22.65	24.80
$(C^{\eta}_{6,-5})^2/\Pi$ (%)	⋯	⋯	0.345	0.668	⋯	0.630	2.732	3.389	1.591
$(C^{\eta}_{7,-6})^2/\Pi$ (%)	⋯	⋯	0.201	0.934	1.332	0.742	0.203	0.190	0.571
$(C^{\eta}_{8,-7})^2/\Pi$ (%)	⋯	⋯	⋯	0.249	0.811	1.129	0.967	0.772	0.475
$(C^{\eta}_{9,-8})^2/\Pi$ (%)	⋯	⋯	⋯	⋯	0.119	0.321	0.295	⋯	0.086
$(C^{\eta}_{-3,4})^2/\Pi$ (%)	⋯	⋯	⋯	⋯	0.092	0.322	0.815	1.362	1.408
$(C^{\eta}_{10,-9})^2/\Pi$ (%)	⋯	⋯	⋯	⋯	⋯	⋯	⋯	0.223	0.758
$(C^{\eta}_{11,-10})^2/\Pi$ (%)	⋯	⋯	⋯	⋯	⋯	⋯	0.072	0.362	0.503
$(C^{\eta}_{12,-11})^2/\Pi$ (%)	⋯	⋯	⋯	⋯	⋯	⋯	⋯	0.117	0.057

detailed components along with the associated coefficients in the initial guess $\varphi_{0,2}$ (61) are listed in Table V in Appendix D. Once a convergent series solution has been obtained by the HAM for each case, the Galerkin iterations then continue based on the series solution to obtain more accurate results. For $\epsilon > 1.008$, we use the Galerkin method to obtain accurate steady-state solutions. Solutions with smaller ϵ are chosen as the initial solutions of the iteration for larger ϵ.

We define $\sigma(m, n) = m\sigma_1 + n\sigma_2$ as the actual angular frequency of component (m, n). Table IV lists the energy distributions of steady-state resonant interfacial waves for ϵ increased up to 1.0147. As ϵ increases, the summed energy proportion containing two primary components occupies less than 10% of the total energy when $\epsilon \geq 1.004$. The energy proportions of the lower frequency components [including $\sigma(2, -1)$, $\sigma(-1, 2)$ and $\sigma(3, -2)$] appear to oscillate with ϵ, whereas the energy proportions of the lowest frequency components $\sigma(-2, 3)$, $\sigma(-3, 4)$ and almost all the remaining high

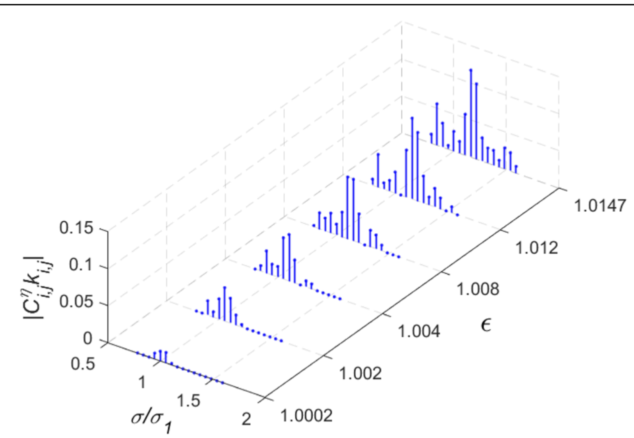

FIG. 6. Discrete dimensionless amplitude spectra $\left|C^{\eta}_{i,j}k_{i,j}\right|$ for steady-state multiple nearly resonant interfacial waves for group S2 in the case of (70).

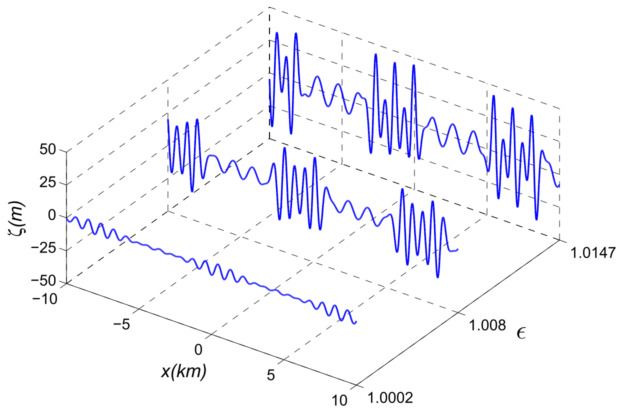

FIG. 7. Spatial profiles of interfacial wave elevation $\zeta(m)$ at $t = 0$ s for group S2 in the case of (70).

frequency components increase monotonically. This indicates that energy is transferred gradually from primary and low frequency components to the lowest frequency components and high frequency components, as the nonlinearity increases. Moreover, the dominant frequency shifts higher as ϵ increases, a finding that concurs with other surface gravity wave situations such as nonlinear sloshing in a rectangular tank where the angular frequency of nonlinear sloshing waves in shallow water increases with nonlinearity [see, e.g., Tadjbakhsh and Keller (1960), Vanden-Broeck and Schwartz (1981), and Tsai and Jeng (1994)].

Figure 6 presents the discrete frequency spectra of dimensionless amplitude $\left|C^{\eta}_{i,j}k_{i,j}\right|$, evaluated for six dimensionless angular frequencies ϵ in the range (1.0002, 1.0147). As ϵ increases, the maximum amplitudes $\left|C^{\eta}_{i,j}k_{i,j}\right|$ increase, and many previously trivial components evolve into the non-trivial ones that must not be neglected in the wave system. This means that increasing numbers of

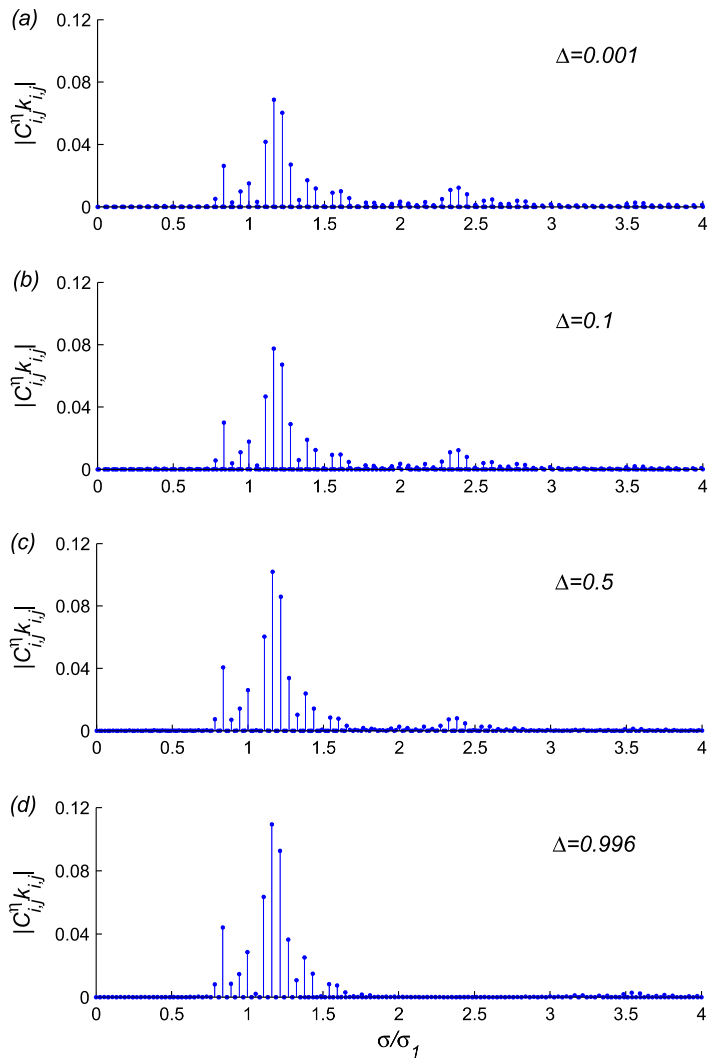

FIG. 8. Discrete spectra of dimensionless amplitude $\left|C^{\eta}_{i,j}k_{i,j}\right|$ for different Δ for group S2 when $h_1/\lambda_2 = 0.5$, $h_2/\lambda_2 = 2$, $\alpha = \pi/36$, and $\epsilon = 1.012$. Wave number ratio k_2/k_1 changes with Δ so that the component (2, −1) corresponds to the exact resonant one.

components participate in the resonance. The frequency band σ/σ_1 broadens as ϵ increases. Moreover, when the nonlinearity is weak (ϵ = 1.0002), a single peak exists in the spectrum. However, when the nonlinearity is stronger, further local peaks appear (growing into sidebands at 4/5 and 3/2 of the primary frequency σ_1). The wave steepness H_s of group 2 increases to 0.28 for ϵ = 1.0147.

Figure 7 plots the interface elevation ζ profile over a distance of 20 km around the crests for three values of dimensionless angular frequency ϵ. The interface profiles exhibit alternating bursts of high frequency, high-amplitude narrow-banded waves followed by lower frequency, lower amplitude waves. Multiple waves of similar height exist in each high-amplitude burst. There is a general growth in wave amplitude with increasing ϵ. For ϵ = 1.0147, the maximum wave height of the calculated interfacial waves reaches 89 m, and the wavelength of the wave group reaches near 8100 m. It is worth mentioning that the maximum wave height and wavelength of the steady-state resonant interface waves match those of internal solitons in the northeastern South China Sea (Ramp *et al.*, 2004). In practice, this would have implications for the movement of stresses on a nuclear-powered submarine traveling at about 500 m below sea level.

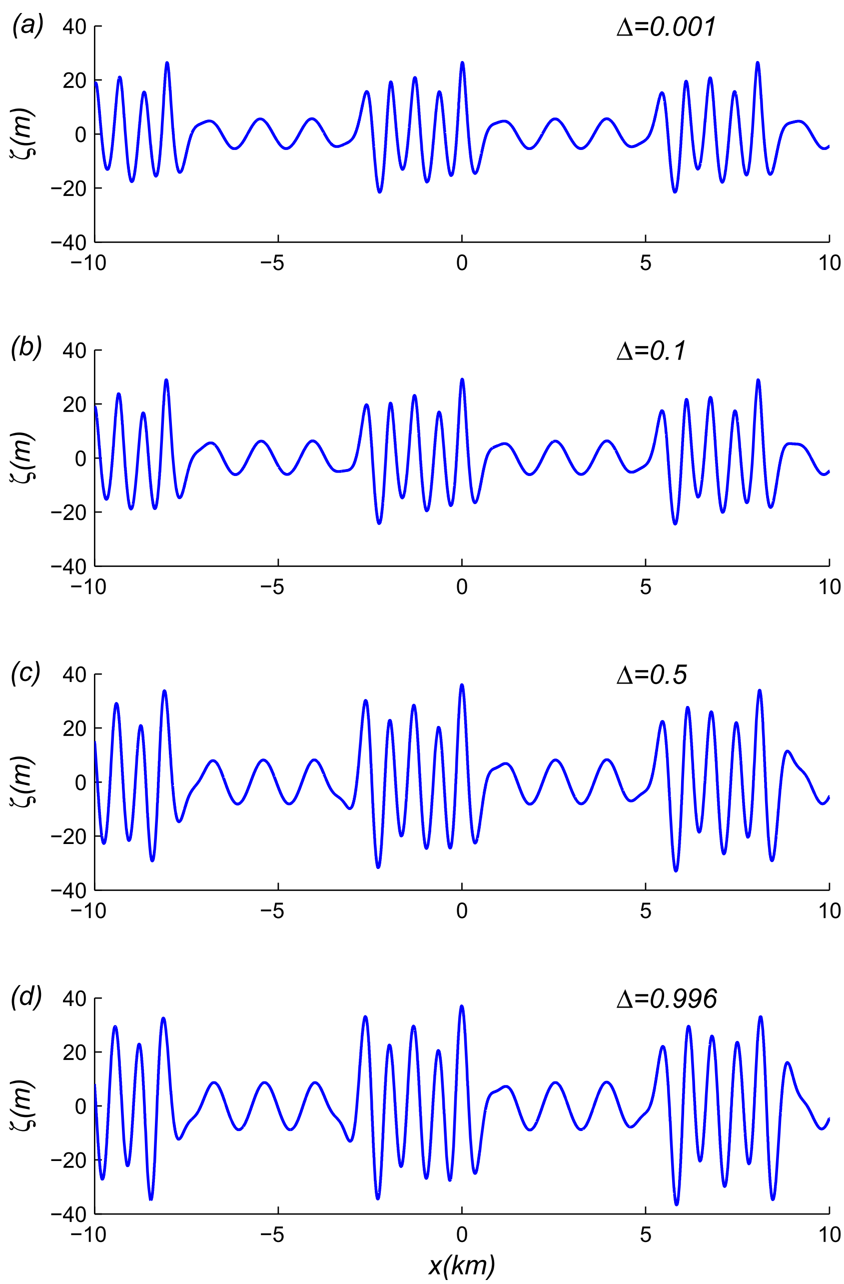

FIG. 9. Interface elevation $\zeta(m)$ profiles over a distance of 20 km about the main crests at t = 0 s for different Δ for group S2 when h_1/λ_2 = 0.5, h_2/λ_2 = 2, $\alpha = \pi/36$, and ϵ = 1.012. Wave number ratio k_2/k_1 changes with Δ so that the component (2, −1) corresponds to the exact resonance.

To summarize, the foregoing has described solutions of steady-state periodic interfacial gravity waves with multiple resonances driven by nonlinearity [as exhibited by the interfacial wave energy spectra (Fig. 6)].

D. Resonant waves with different density ratios

We now examine the influence of density ratio on steady-state near-resonant internal waves. Noting that the fluid densities above and below the interface of a Boussinesq wave are almost identical (Holyer, 1979), we approximate Boussinesq waves by setting $\Delta = 0.996$ and air–water interfacial waves by setting $\Delta = 0.001$. To examine the effect of changing the densities, two other density configurations $\Delta = 0.5$ and $\Delta = 0.1$ are studied here, keeping all other parameters the same.

Figure 8 shows the discrete spectra of dimensionless amplitude $\left|C^{\eta}_{i,j}k_{i,j}\right|$ obtained for interfacial waves with four different density ratios for group S2 when $h_1/\lambda_2 = 0.5$, $h_2/\lambda_2 = 2$, $\alpha = \pi/36$, and $\epsilon = 1.012$. Here, k_2/k_1 is determined so that the component (2, −1) corresponds to the exact resonance for different values of Δ. It is found that the spectra of steady-state resonant interfacial waves change slightly with Δ. The amplitude of high frequency components near $\sigma/\sigma_1 \approx 2.3$ decreases, while the amplitude of components near the primary ones increases. Compared with the Boussinesq wave system, a small part of the total energy is transferred to higher frequency components in the system of air–water interfacial waves. Although changing slightly, the upper layer enlarges the amplitude of components near the primary ones, while lowering the amplitude of higher frequency components.

Figure 9 presents the spatial profiles of the interface elevation ζ for interfacial waves of four different density ratios. Although the shapes of the interface profiles are similar, the maximum wave height increases with Δ. The wave steepness H_s reaches 0.15 and 0.23 for $\Delta = 0.001$ and 0.996, respectively. The upper layer enlarges the wave steepness of interfacial waves as the amplitude of components near the primary ones increases with density ratio.

Figure 10 displays the vertical profiles of the horizontal $x-$ component of velocity for four density ratios. At the density interface, large velocity gradients occur in all four cases. The horizontal velocity of air–water interfacial waves ($\Delta = 0.001$) near the interface is far larger than that of the corresponding Boussinesq waves ($\Delta = 0.996$). In other words, the upper layer reduces the horizontal velocity of the wave field. Although the inviscid model used in this paper inevitably causes a discontinuity in the horizontal velocity component, this would be smeared out in practice, and the foregoing interpretation should nevertheless be useful.

For progressive interfacial waves of finite amplitude, Hunt (1961) found that the principal effect of the upper fluid is to reduce the velocity of propagation and the amplitude of the higher harmonics in the wave profile. Here, we might extend the conclusion of Hunt (1961) from progressive waves with a single primary component to more complicated wave groups with two primary components that contain multiple resonances. More calculations have been conducted for steady-state resonant interfacial waves in groups S1 and S3, and similar conclusions about the effects of density ratio and nonlinearity could be obtained.

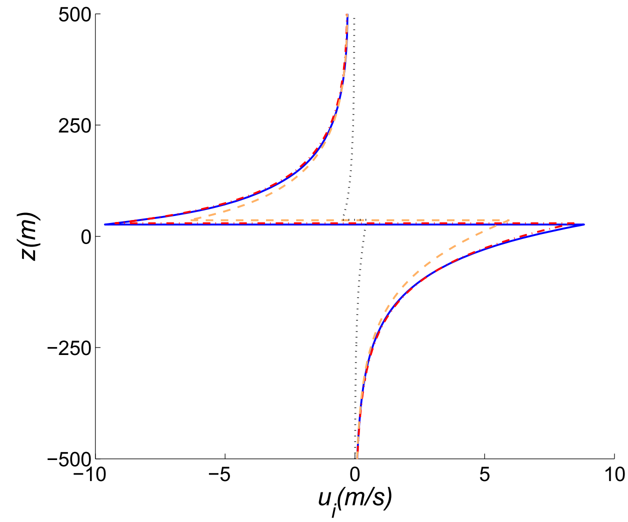

FIG. 10. Vertical profiles of the $x-$ horizontal component of velocity at crests at $t = 0$ s for different Δ corresponding to solution S2 with $h_1/\lambda_2 = 0.5$, $h_2/\lambda_2 = 2$, $\alpha = \pi/36$, and $\epsilon = 1.012$. Wave number ratio k_2/k_1 changes with Δ so that the component (2, −1) corresponds to the exact resonance. Solid line, $\Delta = 0.001$; dashed-dotted line, $\Delta = 0.1$; dashed line, $\Delta = 0.5$; and dotted line, $\Delta = 0.996$.

IV. CONCLUDING REMARKS

Using analytical HAM and a numerical Galerkin's method, we have shown that steady-state periodic interfacial gravity wave solutions can exist under conditions of multiple near resonances for a two-layer fluid filling a frictionless duct with fixed upper and lower boundaries. To achieve this, the fully nonlinear governing equations are solved using the HAM to derive steady-state resonant solutions to a certain level of accuracy and provide initial solutions that are then iterated using Galerkin's method to obtain convergent solutions of sufficient accuracy, according to multiple near resonance criteria. By inserting a piecewise parameter in the auxiliary linear operators and solving the high-order deformation equations simultaneously, the HAM was able to avoid arithmetic problems arising from small denominators and singularities (that afflict the traditional perturbation method).

The physical parameters were chosen so that they approximate actual ocean conditions in the northeastern part of the South China Sea. In the spirit of previous studies by Liao (2011b), Liao *et al.* (2016), Liu *et al.* (2018), and Yang *et al.* (2018), we believe that interfacial waves with time-independent spectra in the ocean may exhibit steady-state resonance in an analogous manner to surface gravity waves and acoustic-gravity waves. It should be noted that steady-state resonant surface waves (air–water interfacial waves) obtained by the HAM in previous studies are particular cases of the more general steady-state resonant interfacial waves considered in the present paper.

For weakly nonlinear interfacial waves with a single exactly resonant quartet, three convergent solutions with different energy distributions are obtained for a system with two primary components and an exactly resonant component. For the three solutions considered herein, the energy related to these components dominates the total energy of the system. Analogous phenomena have previously been found in steady-state surface gravity waves with a single resonant quartet by Liao (2011b), Xu *et al.* (2012), and Liao *et al.* (2016). In addition, for all three solutions, the amplitude of each interfacial wave component tends to increase with density ratio, and the upper layer raises the wave steepness, while reducing the average velocity. Here, the existence of steady-state periodic interfacial gravity waves with a single exactly resonant quartet has been confirmed for the first time.

As nonlinearity increases, the interfacial wave energy spectrum broadens from a small primary peak to the one with a larger primary peak and sideband peaks at frequencies that are 4/5 and 3/2 the primary wave frequency σ_1. The dominant frequency also exhibits a monotonic, though small, increase with nonlinearity. The spectra indicate that previously trivial components can become non-trivial as nonlinearity increases and so cannot be neglected in the wave system as further components participate in resonance. At all levels of nonlinearity considered, the steady-state interfacial wave profile comprises two types of waves that appear in a repeating consecutive pattern: high (nearly constant) amplitude, high frequency waves followed by low (again nearly constant) amplitude, low frequency waves. Our results prove the theoretical existence of steady-state periodic interfacial gravity waves with multiple resonances.

We also confirm the existence of steady-state resonant interfacial waves of finite amplitude at other density ratios. It has been found that, though changing slightly, the upper layer might reduce the amplitude of high frequency components, while increasing the amplitude of components near the primary one. In addition, the upper layer increases the wave steepness of interfacial waves and decreases the horizontal velocity of the wave field. Hunt (1961) finding that the presence of an upper fluid layer reduces the propagation velocity and the amplitude of higher harmonics in the wave profile, may be extended from progressive waves with a single primary component to more complicated wave groups with two primary components that contain multiple resonances.

In this work, the depth of the upper fluid layer is sufficiently large that we ignored the influence of the free surface on the interface. Interactions between surface and interfacial waves in a shallower upper fluid layer will be considered in the future. Besides, we considered steady-state resonant interfacial wave groups with discrete wave spectra. Extension from discrete to continuous spectra will also be considered.

ACKNOWLEDGMENTS

The authors are grateful to the anonymous reviewers for their valuable comments and suggestions that enhanced the quality of this article. This work was partly supported by the National Natural Science Foundation of China (Approval Nos. 51609090 and 11432009) and the State Key Laboratory of Ocean Engineering of China (Approval No. 1806).

APPENDIX A: DERIVATION OF INTERFACE CONDITIONS

The interface elevation ζ is obtained by solving Eq. (9) to give

$$\zeta = \frac{1}{g(\rho_2-\rho_1)}\left[\rho_1\left(\frac{\partial\phi_1}{\partial t}+\frac{1}{2}|\nabla\phi_1|^2\right) - \rho_2\left(\frac{\partial\phi_2}{\partial t}+\frac{1}{2}|\nabla\phi_2|^2\right)\right] \quad \text{at } z=\zeta. \tag{A1}$$

Carrying out partial differentiation of (A1) with respect to x, y, and t, and substituting into Eqs. (7) and (8), ζ is then eliminated to give

$$\rho_2\frac{\partial^2\phi_2}{\partial t^2}+g(\rho_2-\rho_1)\frac{\partial\phi_2}{\partial z}-\rho_1\frac{\partial^2\phi_1}{\partial t^2}+\rho_2\frac{\partial(|\nabla\phi_2|^2)}{\partial t} - \rho_1\frac{\partial(\frac{1}{2}|\nabla\phi_1|^2)}{\partial t}+\rho_2\nabla\phi_2\cdot\nabla\left(\frac{1}{2}|\nabla\phi_2|^2\right) - \rho_1\nabla\phi_2\cdot\nabla\left(\frac{\partial\phi_1}{\partial t}+\frac{1}{2}|\nabla\phi_1|^2\right)=0 \quad \text{at } z=\zeta, \tag{A2}$$

$$\rho_2\frac{\partial^2\phi_2}{\partial t^2}+g(\rho_2-\rho_1)\frac{\partial\phi_1}{\partial z}-\rho_1\frac{\partial^2\phi_1}{\partial t^2}-\rho_1\frac{\partial(|\nabla\phi_1|^2)}{\partial t} +\rho_2\frac{\partial(\frac{1}{2}|\nabla\phi_2|^2)}{\partial t}-\rho_1\nabla\phi_1\cdot\nabla\left(\frac{1}{2}|\nabla\phi_1|^2\right) +\rho_2\nabla\phi_1\cdot\nabla\left(\frac{\partial\phi_2}{\partial t}+\frac{1}{2}|\nabla\phi_2|^2\right)=0 \quad \text{at } z=\zeta. \tag{A3}$$

Subtracting (A3) from (A2), we obtain

$$g(\rho_2-\rho_1)\frac{\partial(\phi_2-\phi_1)}{\partial z}+\sum_{i=1}^{2}\rho_i\left[\frac{\partial(\frac{1}{2}|\nabla\phi_i|^2)}{\partial t} +\nabla\phi_i\cdot\nabla\left(\frac{1}{2}|\nabla\phi_i|^2\right)\right]-\rho_1\nabla\phi_2\cdot\nabla\left(\frac{\partial\phi_1}{\partial t}+\frac{1}{2}|\nabla\phi_1|^2\right) -\rho_2\nabla\phi_1\cdot\nabla\left(\frac{\partial\phi_2}{\partial t}+\frac{1}{2}|\nabla\phi_2|^2\right)=0 \quad \text{at } z=\zeta. \tag{A4}$$

Subsequent derivation is then based on the interface conditions (A1), (A2), and (A4). After transformation [(11) and (12)], the dynamic interface condition (A1) becomes

$$\mathcal{N}_3[\varphi_1,\varphi_2,\eta]=\eta-\frac{1}{g(1-\Delta)}\left[\sum_{i=1}^{2}\sigma_i\frac{\partial\varphi_2}{\partial\xi_i}-f_2 -\Delta\Big(\sum_{i=1}^{2}\sigma_i\frac{\partial\varphi_1}{\partial\xi_i}-f_1\Big)\right]=0, \tag{A5}$$

the kinematic interface condition (A2) becomes

$$\mathcal{N}_1[\varphi_1,\varphi_2]=\sum_{i=1}^{2}\sum_{j=1}^{2}\sigma_i\sigma_j\frac{\partial^2\varphi_2}{\partial\xi_i\partial\xi_j}+g(1-\Delta)\frac{\partial\varphi_2}{\partial z} -\Delta\sum_{i=1}^{2}\sum_{j=1}^{2}\sigma_i\sigma_j\frac{\partial^2\varphi_1}{\partial\xi_i\partial\xi_j}+\widehat{\nabla}\varphi_2\cdot\widehat{\nabla}f_2 -2\sum_{i=1}^{2}\sigma_i\frac{\partial f_2}{\partial\xi_i}+\Delta\left(\sum_{i=1}^{2}\sigma_i\frac{\partial f_1}{\partial\xi_i} -h_{21}-\widehat{\nabla}\varphi_2\cdot\widehat{\nabla}f_1\right)=0, \tag{A6}$$

and another kinematic interface condition (A4) becomes

$$\mathcal{N}_2[\varphi_1,\varphi_2] = g(1-\Delta)\frac{\partial(\varphi_2-\varphi_1)}{\partial z} + \widehat{\nabla}(\varphi_2-\varphi_1)\cdot\widehat{\nabla}f_2 - h_{12} - \sum_{i=1}^{2}\sigma_i\frac{\partial f_2}{\partial \xi_i} - \Delta\left[\sum_{i=1}^{2}\sigma_i\frac{\partial f_1}{\partial \xi_i} + h_{21} + \widehat{\nabla}(\varphi_2-\varphi_1)\cdot\widehat{\nabla}f_1\right] = 0. \tag{A7}$$

The three interface conditions (A5)–(A7) are all satisfied at the unknown interface $z = \eta(\xi_1,\xi_2)$.

APPENDIX B: EXPRESSIONS OF HIGH-ORDER DEFORMATION EQUATIONS IN HAM

Substituting the series (30) and (31) into the zeroth-order deformation equations (27)–(29) with $z = \check{\eta}$, then equating like powers of q, results in the following three linear equations (which we call the high-order deformation equations):

$$\overline{\mathcal{L}}_i[\varphi_{m,1},\varphi_{m,2}] = c_0\Delta^{\varphi}_{m-1,i} + \chi_m(S_{m-1,i} - \overline{S}_{m,i}), \quad i = 1,2, \quad m \ge 1, \tag{B1}$$

$$\eta_m = c_0\Delta^{\eta}_{m-1} + \chi_m\eta_{m-1}, \quad m \ge 1, \tag{B2}$$

where

$$\Delta^{\varphi}_{m,1} = \sigma_1^2\bar{\phi}_m^{2,0,2} + 2\sigma_1\sigma_2\bar{\phi}_m^{1,1,2} + \sigma_2^2\bar{\phi}_m^{0,2,2} + g(1-\Delta)\bar{\phi}_{z,m}^{0,0,2} - \Delta\left(\sigma_1^2\bar{\phi}_m^{2,0,1} + 2\sigma_1\sigma_2\bar{\phi}_m^{1,1,1} + \sigma_2^2\bar{\phi}_m^{0,2,1}\right) + \Lambda^{2,2}_{m,1} - 2\left(\sigma_1\Gamma^2_{m,1} + \sigma_2\Gamma^2_{m,2}\right) + \Delta\left(\sigma_1\Gamma^1_{m,1} + \sigma_2\Gamma^1_{m,2} - \Lambda^{2,1}_{m,2} - \Lambda^{2,1}_{m,1}\right), \tag{B3}$$

$$\Delta^{\varphi}_{m,2} = g(1-\Delta)\left(\bar{\phi}_{z,m}^{0,0,2} - \bar{\phi}_{z,m}^{0,0,1}\right) - \sigma_1\Gamma^2_{m,1} - \sigma_2\Gamma^2_{m,2} + \Lambda^{2,2}_{m,1} - \Lambda^{1,2}_{m,2} - \Lambda^{1,2}_{m,1} + \Delta\left(\Lambda^{1,1}_{m,1} - \Lambda^{2,1}_{m,2} - \Lambda^{2,1}_{m,1} - \sigma_1\Gamma^1_{m,1} - \sigma_2\Gamma^1_{m,2}\right), \tag{B4}$$

$$\Delta^{\eta}_m = \eta_m + \frac{1}{g(1-\Delta)}\left[\Gamma^2_{m,0} - \sigma_1\bar{\phi}_m^{1,0,2} - \sigma_2\bar{\phi}_m^{0,1,2} + \Delta\left(\sigma_1\bar{\phi}_m^{1,0,1} + \sigma_2\bar{\phi}_m^{0,1,1} - \Gamma^1_{m,0}\right)\right], \tag{B5}$$

where

$$\Gamma^k_{m,0} = \sum_{n=0}^{m}\left(\frac{k_1^2}{2}\bar{\phi}_n^{1,0,k}\bar{\phi}_{m-n}^{1,0,k} + \boldsymbol{k}_1\cdot\boldsymbol{k}_2\bar{\phi}_n^{1,0,k}\bar{\phi}_{m-n}^{0,1,k} + \frac{k_2^2}{2}\bar{\phi}_n^{0,1,k}\bar{\phi}_{m-n}^{0,1,k} + \frac{1}{2}\bar{\phi}_{z,n}^{0,0,k}\bar{\phi}_{z,m-n}^{0,0,k}\right), \quad k = 1,2, \tag{B6}$$

$$\Gamma^k_{m,1} = \sum_{n=0}^{m}\left[k_1^2\bar{\phi}_n^{1,0,k}\bar{\phi}_{m-n}^{2,0,k} + \boldsymbol{k}_1\cdot\boldsymbol{k}_2\times\left(\bar{\phi}_n^{1,0,k}\bar{\phi}_{m-n}^{1,1,k} + \bar{\phi}_n^{2,0,k}\bar{\phi}_{m-n}^{0,1,k}\right) + k_2^2\bar{\phi}_n^{0,1,k}\bar{\phi}_{m-n}^{1,1,k} + \bar{\phi}_{z,n}^{0,0,k}\bar{\phi}_{z,m-n}^{1,0,k}\right], \quad k = 1,2, \tag{B7}$$

$$\Gamma^k_{m,2} = \sum_{n=0}^{m}\left[k_1^2\bar{\phi}_n^{1,0,k}\bar{\phi}_{m-n}^{1,1,k} + \boldsymbol{k}_1\cdot\boldsymbol{k}_2\times\left(\bar{\phi}_n^{1,0,k}\bar{\phi}_{m-n}^{0,2,k} + \bar{\phi}_n^{0,1,k}\bar{\phi}_{m-n}^{1,1,k}\right) + k_2^2\bar{\phi}_n^{0,1,k}\bar{\phi}_{m-n}^{0,2,k} + \bar{\phi}_{z,n}^{0,0,k}\bar{\phi}_{z,m-n}^{0,1,k}\right], \quad k = 1,2, \tag{B8}$$

$$\Gamma^k_{m,3} = \sum_{n=0}^{m}\left[k_1^2\bar{\phi}_n^{1,0,k}\bar{\phi}_{z,m-n}^{1,0,k} + \boldsymbol{k}_1\cdot\boldsymbol{k}_2\times\left(\bar{\phi}_n^{1,0,k}\bar{\phi}_{z,m-n}^{0,1,k} + \bar{\phi}_n^{0,1,k}\bar{\phi}_{z,m-n}^{1,0,k}\right) + k_2^2\bar{\phi}_n^{0,1,k}\bar{\phi}_{z,m-n}^{0,1,k} + \bar{\phi}_{z,n}^{0,0,k}\bar{\phi}_{zz,m-n}^{0,0,k}\right], \quad k = 1,2, \tag{B9}$$

$$\Lambda^{i,j}_{m,1} = \sum_{n=0}^{m}\left[k_1^2\bar{\phi}_n^{1,0,i}\Gamma^j_{m-n,1} + \boldsymbol{k}_1\cdot\boldsymbol{k}_2\times\left(\bar{\phi}_n^{1,0,i}\Gamma^j_{m-n,2} + \bar{\phi}_n^{0,1,i}\Gamma^j_{m-n,1}\right) + k_2^2\bar{\phi}_n^{0,1,i}\Gamma^j_{m-n,2} + \bar{\phi}_{z,n}^{0,0,i}\Gamma^j_{m-n,3}\right], \quad i,j = 1,2, \tag{B10}$$

$$\Lambda^{i,j}_{m,2} = -\sigma_1\sum_{n=0}^{m}\left[k_1^2\bar{\phi}_n^{1,0,i}\bar{\phi}_{m-n}^{2,0,j} + \boldsymbol{k}_1\cdot\boldsymbol{k}_2\times\left(\bar{\phi}_n^{1,0,i}\bar{\phi}_{m-n}^{1,1,j} + \bar{\phi}_n^{0,1,i}\bar{\phi}_{m-n}^{2,0,j}\right) + k_2^2\bar{\phi}_n^{0,1,i}\bar{\phi}_{m-n}^{1,1,j} + \bar{\phi}_{z,n}^{0,0,i}\bar{\phi}_{z,m-n}^{1,0,j}\right] - \sigma_2\sum_{n=0}^{m}\left[k_1^2\bar{\phi}_n^{1,0,i}\bar{\phi}_{m-n}^{1,1,j} + k_2^2\bar{\phi}_n^{0,1,i}\bar{\phi}_{m-n}^{0,2,j} + \bar{\phi}_{z,n}^{0,0,i}\bar{\phi}_{z,m-n}^{0,1,j} + \boldsymbol{k}_1\cdot\boldsymbol{k}_2\times\left(\bar{\phi}_n^{1,0,i}\bar{\phi}_{m-n}^{0,2,j} + \bar{\phi}_n^{0,1,i}\bar{\phi}_{m-n}^{1,1,j}\right)\right], \quad i,j = 1,2, \tag{B11}$$

$$\mu_{m,n} = \begin{cases} \eta_n, & m = 1, \quad n \ge 1 \\ \sum_{i=m-1}^{n-1}\mu_{m-1,i}\eta_{n-i}, & m \ge 2, \quad n \ge m, \end{cases} \tag{B12}$$

$$\psi^{n,m}_{i,j,k} = \frac{\partial^{i+j}}{\partial\xi_1^i\partial\xi_2^j}\left(\frac{1}{m!}\frac{\partial^m\varphi_{n,k}}{\partial z^m}\bigg|_{z=0}\right), \quad k = 1,2, \tag{B13}$$

$$\beta^{n,m}_{i,j,k} = \begin{cases} \psi^{n,0}_{i,j,k}, & m = 0 \\ \sum_{s=1}^{m}\psi^{n,s}_{i,j,k}\mu_{s,m}, & m \ge 1, \end{cases} \tag{B14}$$

$$\gamma^{n,m}_{i,j,k} = \begin{cases} \psi^{n,1}_{i,j,k}, & m = 0 \\ \sum_{s=1}^{m}(s+1)\psi^{n,s+1}_{i,j,k}\mu_{s,m}, & m \ge 1, \end{cases} \tag{B15}$$

$$\delta_{i,j,k}^{n,m} = \begin{cases} 2\psi_{i,j,k}^{n,2}, & m = 0 \\ \sum_{s=1}^{m}(s+1)(s+2)\psi_{i,j,k}^{n,s+2}\mu_{s,m}, & m \geq 1, \end{cases} \tag{B16}$$

$$\bar{\phi}_{n}^{i,j,k} = \sum_{m=0}^{n}\beta_{i,j,k}^{n-m,m}, \quad \bar{\phi}_{z,n}^{i,j,k} = \sum_{m=0}^{n}\gamma_{i,j,k}^{n-m,m}, \quad \bar{\phi}_{zz,n}^{i,j,k} = \sum_{m=0}^{n}\delta_{i,j,k}^{n-m,m}. \tag{B17}$$

The linear operators are prescribed such that $\overline{\mathcal{L}}_1 = \mathcal{L}_1|_{z=0}$ and $\overline{\mathcal{L}}_2 = \mathcal{L}_2|_{z=0}$. The expressions for $\mathcal{L}_i$, $S_{m-1,i}$, and $\overline{S}_{m,i}$, with $i = 1, 2$, are given in Sec. II B 2.

APPENDIX C: DETAILED DERIVATION OF THE JACOBIAN MATRICES

The Jacobian matrices, including $\partial P_{r,s}/\partial C_{i,j}^{\varphi_1}$, $\partial P_{r,s}/\partial C_{i,j}^{\varphi_2}$, $\partial Q_{r,s}/\partial C_{i,j}^{\varphi_1}$, $\partial Q_{r,s}/\partial C_{i,j}^{\varphi_2}$, and $\partial R_{r,s}/\partial C_{i,j}^{\eta}$, are given by

$$\frac{\partial P_{r,s}}{\partial C_{i,j}^{\varphi_1}} = \int_0^{2\pi}\int_0^{2\pi}\left(\frac{\partial \mathcal{N}_1}{\partial C_{i,j}^{\varphi_1}} + \frac{\partial \mathcal{N}_1}{\partial z}\frac{\partial \eta}{\partial C_{i,j}^{\varphi_1}}\right)\sin(r\xi_1 + s\xi_2)d\xi_1 d\xi_2, \tag{C1}$$

$$\frac{\partial P_{r,s}}{\partial C_{i,j}^{\varphi_2}} = \int_0^{2\pi}\int_0^{2\pi}\left(\frac{\partial \mathcal{N}_1}{\partial C_{i,j}^{\varphi_2}} + \frac{\partial \mathcal{N}_1}{\partial z}\frac{\partial \eta}{\partial C_{i,j}^{\varphi_2}}\right)\sin(r\xi_1 + s\xi_2)d\xi_1 d\xi_2, \tag{C2}$$

$$\frac{\partial Q_{r,s}}{\partial C_{i,j}^{\varphi_1}} = \int_0^{2\pi}\int_0^{2\pi}\left(\frac{\partial \mathcal{N}_2}{\partial C_{i,j}^{\varphi_1}} + \frac{\partial \mathcal{N}_2}{\partial z}\frac{\partial \eta}{\partial C_{i,j}^{\varphi_1}}\right)\sin(r\xi_1 + s\xi_2)d\xi_1 d\xi_2, \tag{C3}$$

$$\frac{\partial Q_{r,s}}{\partial C_{i,j}^{\varphi_2}} = \int_0^{2\pi}\int_0^{2\pi}\left(\frac{\partial \mathcal{N}_2}{\partial C_{i,j}^{\varphi_2}} + \frac{\partial \mathcal{N}_2}{\partial z}\frac{\partial \eta}{\partial C_{i,j}^{\varphi_2}}\right)\sin(r\xi_1 + s\xi_2)d\xi_1 d\xi_2, \tag{C4}$$

$$\frac{\partial R_{r,s}}{\partial C_{i,j}^{\eta}} = \int_0^{2\pi}\int_0^{2\pi}\frac{\partial \mathcal{N}_3[\varphi_1,\varphi_2,z]}{\partial z}\cos(i\xi_1 + j\xi_2)\cos(r\xi_1 + s\xi_2)d\xi_1 d\xi_2, \tag{C5}$$

where the unknowns $\partial\eta/\partial C_{i,j}^{\varphi_1}$ and $\partial\eta/\partial C_{i,j}^{\varphi_2}$ are determined by the equations

$$\frac{\partial \mathcal{N}_3[\varphi_1,\varphi_2,z]}{\partial C_{i,j}^{\varphi_1}} + \frac{\partial \mathcal{N}_3[\varphi_1,\varphi_2,z]}{\partial z}\frac{\partial \eta}{\partial C_{i,j}^{\varphi_1}} = 0, \tag{C6}$$

$$\frac{\partial \mathcal{N}_3[\varphi_1,\varphi_2,z]}{\partial C_{i,j}^{\varphi_2}} + \frac{\partial \mathcal{N}_3[\varphi_1,\varphi_2,z]}{\partial z}\frac{\partial \eta}{\partial C_{i,j}^{\varphi_2}} = 0 \tag{C7}$$

from (17). The expressions for $\mathcal{N}_1$, $\mathcal{N}_2$, and $\mathcal{N}_3$ are as follows:

$$\begin{aligned}\mathcal{N}_1[\varphi_1,\varphi_2] = {} & TF_2{}^2\varphi_{2\xi_1\xi_1} + 2TF_2TS_2\varphi_{2\xi_1\xi_2} + TS_2{}^2\varphi_{2\xi_2\xi_2} \\ & + \varphi_{2z}[2TF_2\varphi_{2\xi_1 z} + 2TS_2\varphi_{2\xi_2 z} + g(1-\Delta) + \varphi_{2z}\varphi_{2zz}] \\ & - \Delta[TF_2TF_1\varphi_{1\xi_1\xi_1} + (TS_1TF_2 + TF_1TS_2)\varphi_{1\xi_1\xi_2} \\ & + TS_2TS_1\varphi_{1\xi_2\xi_2} + (TF_1\varphi_{2z} + TF_2\varphi_{1z})\varphi_{1\xi_1 z} \\ & + (TS_1\varphi_{2z} + TS_2\varphi_{1z})\varphi_{1\xi_2 z} + \varphi_{2z}\varphi_{1z}\varphi_{1zz}],\end{aligned} \tag{C8}$$

$$\begin{aligned}\mathcal{N}_2[\varphi_1,\varphi_2] = {} & [g(1-\Delta) + \varphi_{2z}\varphi_{2zz}]DP_z + TF_2DTF\varphi_{2\xi_1\xi_1} + \big(TS_2DTF \\ & + TF_2DTS\big)\varphi_{2\xi_1\xi_2} + TS_2DTS\varphi_{2\xi_2\xi_2} + \big(DTF\varphi_{2z} + TF_2DP_z\big)\varphi_{2\xi_1 z} \\ & + \big(DTS\varphi_{2z} + TS_2DP_z\big)\varphi_{2\xi_2 z} - \Delta\big[TF_1DTF\varphi_{1\xi_1\xi_1} + \big(TS_1DTF \\ & + TF_1DTS\big)\varphi_{1\xi_1\xi_2} + TS_1DTS\varphi_{1\xi_2\xi_2} + \big(DTF\varphi_{1z} + TF_1DP_z\big)\varphi_{1\xi_1 z} \\ & + \big(DTS\varphi_{1z} + TS_1DP_z\big)\varphi_{1\xi_2 z} + \varphi_{1z}\varphi_{1zz}DP_z\big],\end{aligned} \tag{C9}$$

$$\begin{aligned}\mathcal{N}_3[\varphi_1,\varphi_2,z] = {} & z - \frac{1}{2g(1-\Delta)}\{(\sigma_1 - TF_2)\varphi_{2\xi_1} + (\sigma_2 - TS_2)\varphi_{2\xi_2} \\ & - \varphi_{2z}^2 - \Delta\big[(\sigma_1 - TF_1)\varphi_{1\xi_1} + (\sigma_2 - TS_1)\varphi_{1\xi_2} - \varphi_{1z}^2\big]\},\end{aligned} \tag{C10}$$

where

$$TF_j = k_1^2\varphi_{j\xi_1} + \boldsymbol{k}_1\cdot\boldsymbol{k}_2\varphi_{j\xi_2} - \sigma_1,\ TS_j = k_2^2\varphi_{j\xi_2} + \boldsymbol{k}_1\cdot\boldsymbol{k}_2\varphi_{j\xi_1} - \sigma_2,\ j = 1,2, \tag{C11}$$

$$DTF = TF_2 - TF_1,\ DTS = TS_2 - TS_1,\ DP_z = \varphi_{2z} - \varphi_{1z}. \tag{C12}$$

The formulas for $\partial\mathcal{N}_r/\partial C_{i,j}^{\varphi_1}$, $\partial\mathcal{N}_r/\partial C_{i,j}^{\varphi_2}$ and $\partial\mathcal{N}_r/\partial z$, with $r = 1, 2, 3$, are obtained by direct derivation.

APPENDIX D: DETAILED RESULTS OF INITIAL GUESS IN HAM

In Sec. III B, when $m = 1$, nonlinear algebraic equations (58) about $C_{1,0}^{\varphi_2,0}$, $C_{0,1}^{\varphi_2,0}$, and $C_{2,-1}^{\varphi_2,0}$ have three groups of solutions, as listed in Table V.

In Sec. III C, the detailed components together with the absolute values of the associated coefficients in the initial guess $\varphi_{0,2}$ (61) for group S2 in the case of (70) are listed in Table VI.

TABLE V. The solutions of the nonlinear algebraic equations (58) in the case of (70) with $\epsilon = 1.0002$.

Group	$\lvert C_{1,0}^{\varphi_2,0}\rvert$ (m^2/s)	$\lvert C_{0,1}^{\varphi_2,0}\rvert$ (m^2/s)	$\lvert C_{2,-1}^{\varphi_2,0}\rvert$ (m^2/s)
S1	3.66×10^{-6}	2.76×10^{-5}	3.96×10^{-7}
S2	3.45×10^{-6}	1.35×10^{-5}	5.39×10^{-7}
S3	3.25×10^{-6}	1.05×10^{-5}	1.04×10^{-6}

TABLE VI. Detailed components together with the absolute values of the associated coefficients in the initial guess $\varphi_{0,2}$ (61) for group S2 in the case of (70).

	Dimensionless angular frequency ϵ								
Components of $\varphi_{0,2}$ (m^2/s)	1.0002	1.001	1.002	1.003	1.004	1.005	1.006	1.007	1.008
$\psi^2_{1,0} \times 10^{-6}$	3.45	7.10	9.47	8.21	7.17	5.45	3.42	1.51	0.12
$\psi^2_{0,1} \times 10^{-5}$	1.35	2.13	1.83	0.13	1.13	2.26	3.17	3.84	4.29
$\psi^2_{2,-1} \times 10^{-6}$	0.54	1.36	2.09	2.56	2.87	2.99	2.95	2.84	2.70
$\psi^2_{3,-2} \times 10^{-7}$	…	0.96	1.88	3.29	4.33	5.28	6.06	6.65	7.10
$\psi^2_{-1,2} \times 10^{-4}$	…	0.51	1.13	1.89	2.11	2.17	2.10	1.95	1.77
$\psi^2_{4,-3} \times 10^{-8}$	…	…	…	1.91	2.94	4.28	5.80	7.27	8.59
$\psi^2_{5,-4} \times 10^{-9}$	…	…	…	0.16	0.36	1.00	2.09	3.41	4.75
$\psi^2_{-2,3} \times 10^{-4}$	…	…	…	1.72	2.91	4.11	5.24	6.21	7.02

DATA AVAILABILITY

The data that support the findings of this study are available from the corresponding author upon reasonable request.

REFERENCES

Aghsaee, P., Boegman, L., and Lamb, K. G., "Breaking of shoaling internal solitary waves," J. Fluid Mech. **659**, 289–317 (2010).

Aksel, N. and Schörner, M., "Films over topography: From creeping flow to linear stability, theory, and experiments, a review," Acta Mech. **229**, 1453–1482 (2018).

Akylas, T. R. and Karimi, H. H., "Oblique collisions of internal wave beams and associated resonances," J. Fluid Mech. **711**, 337–363 (2012).

Alam, M.-R., "A new triad resonance between co-propagating surface and interfacial waves," J. Fluid Mech. **691**, 267–278 (2012).

Alam, M.-R., Liu, Y. M., and Yue, D. K. P., "Bragg resonance of waves in a two-layer fluid propagating over bottom ripples. Part I. Perturbation analysis," J. Fluid Mech. **624**, 191–224 (2009).

Alam, M.-R., Liu, Y. M., and Yue, D. K. P., "Oblique sub-and super-harmonic Bragg resonance of surface waves by bottom ripples," J. Fluid Mech. **643**, 437–447 (2010).

Amundsen, D. E., "Resonance in dispersive wave systems," Ph.D. thesis, Massachusetts Institute of Technology, 1999.

Ball, F. K., "Energy transfer between external and internal gravity waves," J. Fluid Mech. **19**, 465–478 (1964).

Benjamin, T. B., "Internal waves of finite amplitude and permanent form," J. Fluid Mech. **25**, 241–270 (1966).

Benjamin, T. B., "Internal waves of permanent form in fluids of great depth," J. Fluid Mech. **29**, 559–592 (1967).

Camassa, R., Rusas, P. O., Saxena, A., and Tiron, R., "Fully nonlinear periodic internal waves in a two-fluid system of finite depth," J. Fluid Mech. **652**, 259–298 (2010).

Chen, M. J. and Forbes, L. K., "Steady periodic waves in a three-layer fluid with shear in the middle layer," J. Fluid Mech. **594**, 157–181 (2008).

Couston, L. A., "Resonant interactions of surface and internal waves with seabed topography," Ph.D. thesis, University of California, Berkeley, 2016.

Dauxois, T., Joubaud, S., Odier, P., and Venaille, A., "Instabilities of internal gravity wave beams," Annu. Rev. Fluid Mech. **50**, 131–156 (2018).

Fan, Z. S., Shi, X. G., Liu, A. K., Liu, H. L., and Li, P. L., "Effects of tidal currents on nonlinear internal solitary waves in the South China Sea," J. Ocean Univ. China **12**, 13–22 (2013).

Garrett, C. and Munk, W., "Space-time scales of internal waves: A progress report," J. Geophys. Res. **80**, 291–297, https://doi.org/10.1029/jc080i003p00291 (1975).

Garrett, C. and Munk, W., "Internal waves in the ocean," Annu. Rev. Fluid Mech. **11**, 339–369 (1979).

Grimshaw, R. and Helfrich, K., "The effect of rotation on internal solitary waves," IMA J. Appl. Math. **77**, 326–339 (2012).

Grimshaw, R. H. J. and Smyth, N., "Resonant flow of a stratified fluid over topography," J. Fluid Mech. **169**, 429–464 (1986).

Heining, C., Bontozoglou, V., Aksel, N., and Wierschem, A., "Nonlinear resonance in viscous films on inclined wavy planes," Int. J. Multiphase Flow **35**, 78–90 (2009).

Holyer, J. Y., "Large amplitude progressive interfacial waves," J. Fluid Mech. **93**, 433–448 (1979).

Hunt, J. N., "Interfacial waves of finite amplitude," Houille Blanche **4**, 515–531 (1961).

Lake, B. M., Yuen, H. C., Rungaldier, H., and Ferguson, W. E., "Nonlinear deep-water waves: Theory and experiment. Part 2. Evolution of a continuous wave train," J. Fluid Mech. **83**, 49–74 (1977).

Leonard, J. J. and Bahr, A., "Autonomous underwater vehicle navigation," in *Springer Handbook of Ocean Engineering* (Springer, 2016), pp. 341–358.

Leonard, J. J., Bennett, A. A., Smith, C. M., and Feder, H. J. S., "Autonomous underwater vehicle navigation," Technical Report MIT Marine Robotics Laboratory Technical Memorandum, 1998.

Liang, Y., Zareei, A., and Alam, M.-R., "Inherently unstable internal gravity waves due to resonant harmonic generation," J. Fluid Mech. **811**, 400–420 (2017).

Liao, S. J., *Beyond Perturbation: Introduction to the Homotopy Analysis Method* (CRC Press, Boca Raton, 2003).

Liao, S. J., *Homotopy Analysis Method in Nonlinear Differential Equations* (Springer-Verlag, New York, 2011a).

Liao, S. J., "On the homotopy multiple-variable method and its applications in the interactions of nonlinear gravity waves," Commun. Nonlinear Sci. Numer. Simul. **16**, 1274–1303 (2011b).

Liao, S. J., Xu, D. L., and Stiassnie, M., "On the steady-state nearly resonant waves," J. Fluid Mech. **794**, 175–199 (2016).

Liu, Z. and Liao, S. J., "Steady-state resonance of multiple wave interactions in deep water," J. Fluid Mech. **742**, 664–700 (2014).

Liu, Z. and Xie, D., "Finite-amplitude steady-state wave groups with multiple near-resonances in finite water depth," J. Fluid Mech. **867**, 348–373 (2019).

Liu, Z., Xu, D. L., Li, J., Peng, T., Alsaedi, A., and Liao, S. J., "On the existence of steady-state resonant waves in experiments," J. Fluid Mech. **763**, 1–23 (2015).

Liu, Z., Xu, D. L., and Liao, S. J., "Mass, momentum, and energy flux conservation between linear and nonlinear steady-state wave groups," Phys. Fluids **29**, 127104 (2017).

Liu, Z., Xu, D. L., and Liao, S. J., "Finite amplitude steady-state wave groups with multiple near resonances in deep water," J. Fluid Mech. **835**, 624–653 (2018).

Madsen, P. A. and Fuhrman, D. R., "Third-order theory for multi-directional irregular waves," J. Fluid Mech. **698**, 304–334 (2012).

Mccomas, C. H. and Bretherton, F. P., "Resonant interaction of oceanic internal waves," J. Geophys. Res. **82**, 1397–1412, https://doi.org/10.1029/jc082i009p01397 (1977).

Okamura, M., "Almost limiting short-crested gravity waves in deep water," J. Fluid Mech. **646**, 481–503 (2010).

Osborne, A. R. and Burch, T. L., "Internal solitons in the Andaman Sea," Science **208**, 451–460 (1980).

Parau, E. and Dias, F., "Interfacial periodic waves of permanent form with free-surface boundary conditions," J. Fluid Mech. **437**, 325–336 (2001).

Phillips, O. M., "On the dynamics of unsteady gravity waves of finite amplitude. Part 1. The elementary interactions," J. Fluid Mech. **9**, 193–217 (1960).

Ramp, S. R., Tang, T. Y., Duda, T. F., Lynch, J. F., Liu, A. K., Chiu, C. S., Bahr, F. L., Kim, H. R., and Yang, Y. J., "Internal solitons in the Northeastern South China Sea. Part I: Sources and deep water propagation," IEEE J. Oceanic Eng. **29**, 1157–1181 (2004).

Saffman, P. G. and Yuen, H. C., "Finite-amplitude interfacial waves in the presence of a current," J. Fluid Mech. **123**, 459–476 (1982).

Schörner, M., Reck, D., and Aksel, N., "Does the topography's specific shape matter in general for the stability of film flows?," Phys. Fluids **27**, 042103 (2015).

Sutherland, B. R., *Internal Gravity Waves* (Cambridge University Press, 2010).

Tadjbakhsh, I. and Keller, J. B., "Standing surface waves of finite amplitude," J. Fluid Mech. **8**, 442–451 (1960).

Tanaka, M. and Wakayama, K., "A numerical study on the energy transfer from surface waves to interfacial waves in a two-layer fluid system," J. Fluid Mech. **763**, 202–217 (2015).

Thorpe, S. A., "On wave interactions in a stratified fluid," J. Fluid Mech. **24**, 737–751 (1966).

Tsai, C. P. and Jeng, D. S., "Numerical Fourier solutions of standing waves in finite water depth," Appl. Ocean Res. **16**, 185–193 (1994).

Vajravelu, K. and Van Gorder, R. A., *Nonlinear Flow Phenomena and Homotopy Analysis: Fluid Flow and Heat Transfer* (Springer-Verlag, Heidelberg, 2012).

Vanden-Broeck, J. M. and Schwartz, L. W., "Numerical calculation of standing waves in water of arbitrary uniform depth," Phys. Fluids **24**, 812–815 (1981).

Wen, F., "Resonant generation of internal waves on the soft sea bed by a surface water wave," Phys. Fluids **7**, 1915–1922 (1995).

Wierschem, A., Bontozoglou, V., Heining, C., Uecker, H., and Aksel, N., "Linear resonance in viscous films on inclined wavy planes," Int. J. Multiphase Flow **34**, 580–589 (2008).

Xu, D. L., Lin, Z. L., Liao, S. J., and Stiassnie, M., "On the steady-state fully resonant progressive waves in water of finite depth," J. Fluid Mech. **710**, 379–418 (2012).

Yang, X. Y., Dias, F., and Liao, S. J., "On the steady-state resonant acoustic-gravity waves," J. Fluid Mech. **849**, 111–135 (2018).

Zaleski, J., Zaleski, P., and Lvov, Y. V., "Excitation of interfacial waves via surface-interfacial wave interactions," J. Fluid Mech. **887**, A14 (2020).

Zhang, H. P., King, B., and Swinney, H. L., "Resonant generation of internal waves on a model continental slope," Phys. Rev. Lett. **100**, 244504 (2008).